Bistatic Synthetic Aperture Radar imaging based on Geostationary Transmitters and Ground-Based Receivers

Master Thesis

Author: Ricard Pinar Riasol

Supervisor: Dr. Antoni Broquetas Ibars

March 2017

ABSTRACT

This thesis belongs to the remote sensing field, particularly on the Geostationary Synthetic Aperture Radar (SAR) imaging systems with on-ground receiver. These systems forms images taking the signals along the orbital track of one satellite while the receiver is placed on the Earth coherently processing the echoes received by the receiver.

The study presented in this thesis is centered in an algorithm known as back projection algorithm that presents the main advantage that is possible to permanently acquire images from the same region thanks to the small motion of the platform with respect to the Earth.

An introduction to all the important aspects of the GEOSAR mission is presented in order to let the reader known all the important information of why it is important to study the Synthetic Aperture Radars (SAR) mounted on geostationary satellite platforms.

Moreover, an introduction to orbits, coordinates systems and Synthetic Aperture Radar (SAR) is essential in order to understand the algorithm developed in this thesis for obtaining SAR images from a geostationary orbit with the receiver placed on ground. So a detailed explanation of all this topics is developed during this thesis.

The main section of this thesis presents the development of a back projection algorithm for a GEOSAR satellite with on ground receiver. Detailed explanations on how each block of the algorithm has been developed and which are the main functionalities of each block are explained and analysed.

Finally, a test in order to prove that the algorithm works as expected has been performed in order to see if it is possible to obtain SAR images from a geostationary orbit using this geometry.

ACKWONLEDGMENTS:

First of all I would like to thank my master thesis advisor, Dr. Antoni Broquetas Ibars who has always helped me with the doubts and have try to clarify many aspects based on Synthetic Aperture Radars and imaging algorithms.

CONTENTS

LIST OF FIGURES

1. GEOSAR MISSION:

1.1. INTRODUCTION:

Geostationary Synthetic Aperture Radar (GEOSAR) missions are presently being studied in order to provide continuous monitoring of the Earth on a continental scale (Tomiyasu, 1983). Nowadays, LEOSAR (Low Earth Orbit Synthetic Aperture Radar) missions offer Earth imaging, but they cannot provide continuous information about events that suffers rapid changes in short periods of time (LEO satellites have a revisit time of 11-14 days). This permanent monitoring will allow GEOSAR missions to cover a new set of applications, that we will show later in this chapter (Wadge et al, 2014).

The basics of GEOSAR missions are based on a radar payload located in a communication satellite, orbiting on a geostationary orbit. The common think is that a satellite placed on a geostationary orbit remains fixed on the same sky position for an Earth observer. However, this is not strictly true, residual inclination and eccentricity of the satellite orbit results in a small elliptical motion relative to Earth. This fact is crucial for obtaining images from the synthetic aperture.

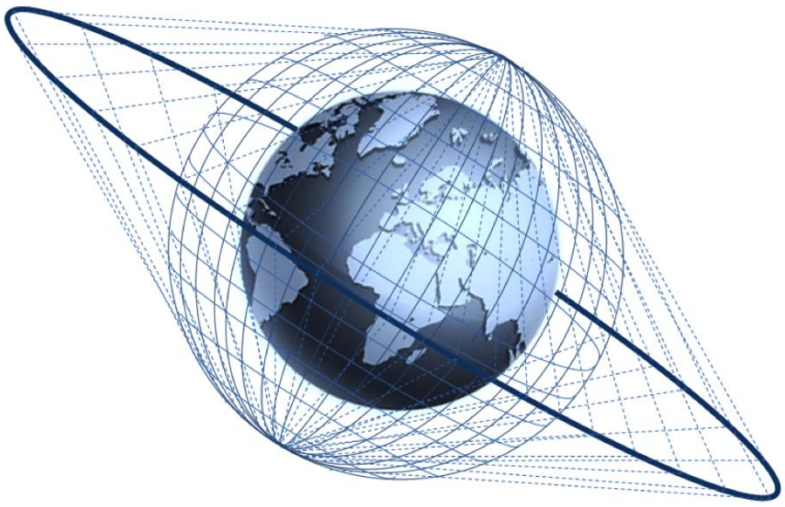

Figure 1: Author's artistic impression of LEO-GEO Hybrid Multigrid Network.

1.2. GEOSAR APPLICATIONS:

The main application (which results also the main advantage) of geostationary radars is the ability to provide early warning and monitor short-lived (less than a day) phenomena that would otherwise be missed, aliased or confused with noise. Some of these short-lived phenomena represent hazards at the Earth's surface (e.g., volcanic eruptions, earthquakes, flooding), and others may be hazardous only at certain times (e.g., landslides, urban subsidence). On the other side, there are other phenomena that do not represent a potential risk for the Earth's surface, but it is important to obtain some valuable information of them within short time intervals (e.g., agricultural events, snow mass).

The main applications of the GEOSAR mission will be explained on the following lines.

1. *Atmospheric Phase Screen (APS)*

   Atmospheric Phase Screen (APS) is a phase alteration on the signals propagated through the atmosphere induced by inhomogeneities in refractive index resulting from changes in pressure, temperature, water vapour content or electron density of the ionosphere. Changes in atmospheric properties (for example, water vapor content, temperature or pressure) provoke variations on the APS. These changes provoke a variation on the atmospheric refractivity index (mostly in the tropospheric layer), and produce an undesired atmospheric phase delay.

   In LEOSAR missions, the integration time is around 1s, which is important in order to consider the APS invariant during the acquisition. However, in GEOSAR missions, the integration time lasts hours, so we cannot consider the APS invariant during the acquisition. APS in GEOSAR missions should be characterized and compensated from the acquired raw data in order to avoid image defocusing.

2. Agriculture

Field-to-field comparisons when farming activities will be provided by using geostationary radar. Such data would feed into farming-centric concerns and management on the one hand, and land surface vegetation models and hydrological small catchment-scale models on the other.

3. Cryosphere

The motion of glaciers can be measured by the advance or retreat of the glacier front and by vectors of motions on the flow surface. Note that many glaciers move some meters on a single day, and that cannot be monitored by LEO satellites due to the high revisit time. So the fact that the Geostationary Satellites have a much shorter revisit time, make it feasible to study the fast motion of glaciers.

With two radars using different frequencies, the snow mass can also be estimated. They could be used together in order to retrieve the mass of dry snow and the location of the region over which the snow was melting.

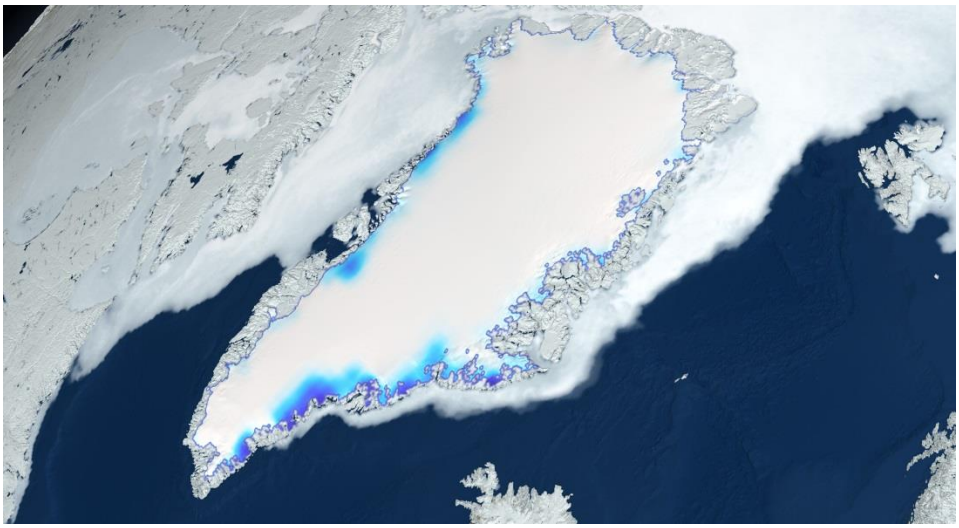

Figure 2: shades of blue portray a reduction in the elevation of the Greenland ice sheet as measured by the ICESat satellite between 2003 and 2006.

4. *Earthquakes*

One of the remarkable characteristics of Synthetic Aperture Radar (SAR) is to record physical value called the backscattering coefficient of the Earth's surface not depending on weather conditions and Sun illumination. Therefore, SAR could be a powerful tool and be used to develop a universal method for grasping damaged areas by disasters such as earthquakes, forest fires and floods.

5. *Flooding*

Flood monitoring using geostationary satellite data should be an effective method to get quick and precise overview of flooded areas. Images showing the flood boundary every 2 hours would be a major advantage on current and planned capabilities, though they would not be available at all times.

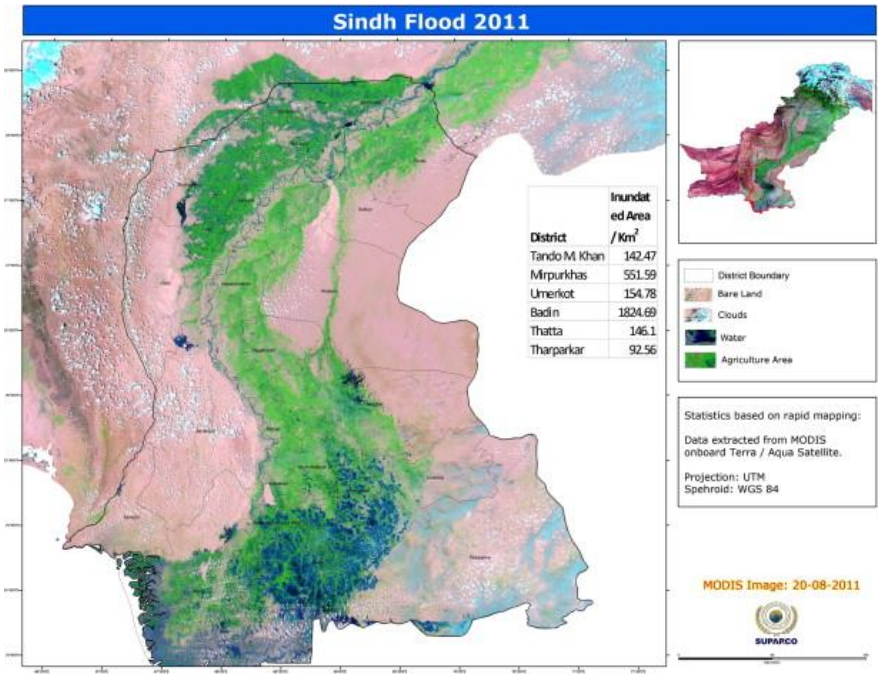

Figure 3: MODIS image showing the inundated area on Aug 20, 2011.

6. *Hydrology*

An essential climate variable is the soil moisture, and some satellites are especially dedicated to its measurement. However, the high revisit time makes it infrequent to measure and that provokes a lack of quality in the measurement or precipitation events. A backscatter-based retrieval of soil moisture at a scale of 1km/1 h is required to do this. To sum up, continuous monitoring must be used.

7. *Landslides*

The fact that using a GEOSAR satellite we are able to monitor continuously the soil displacements is useful for assessing and preventing landslides. Note that local landslides can be monitored using a ground-based Interferometric Synthetic Aperture Radar but regional or continental surveillance requires satellite-based methods.

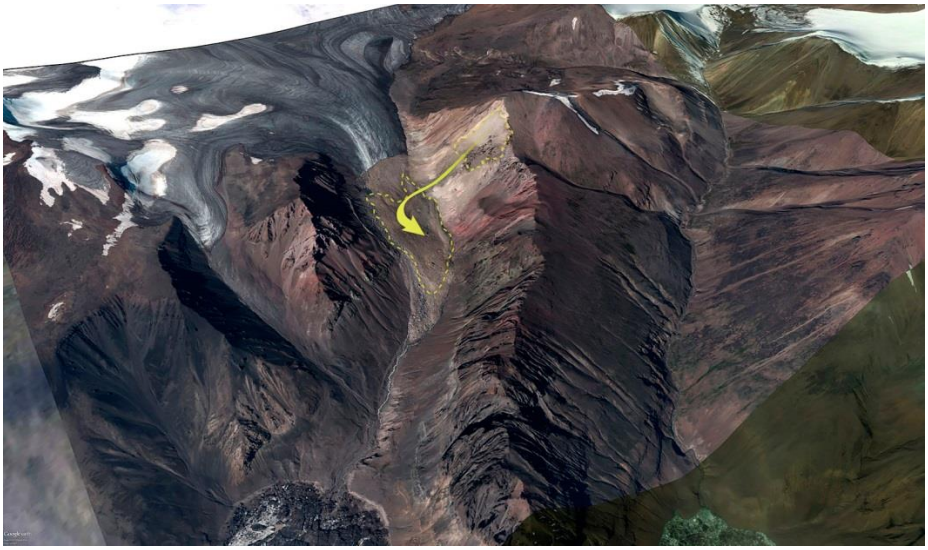

Figure 4: A satellite view shows a landslide in Alaska, with yellow indicating its direction. The debris field (outlined by the dotted yellow line) buried part of a glacier.

8. Volcanoes

To understand the location, motion and threat posed of lava flows, pyroclastic flows and ash falls is vital to advice the civil authorities on evacuations and other mitigation measures. Note that LEO satellites are not able to monitor the complex pattern of deformation that magma makes before and during an eruption.

1.3. L-BAND AND X-BAND RADARS:

A dual band GEOSAR mission has been recently proposed: one working at L-band and the other at X-band (Wadge et al., 2014).

The L-band wide coverage beam will offer continental coverage (approximately 3000 km) with 1 km resolution and taking an integration time of approximately 20 to 30 minutes. On the other hand, the X-band radar will be used to cover smaller areas (approximately 500 km), with observation times of some hours and we will obtain medium resolution images (10 to 20 meters).

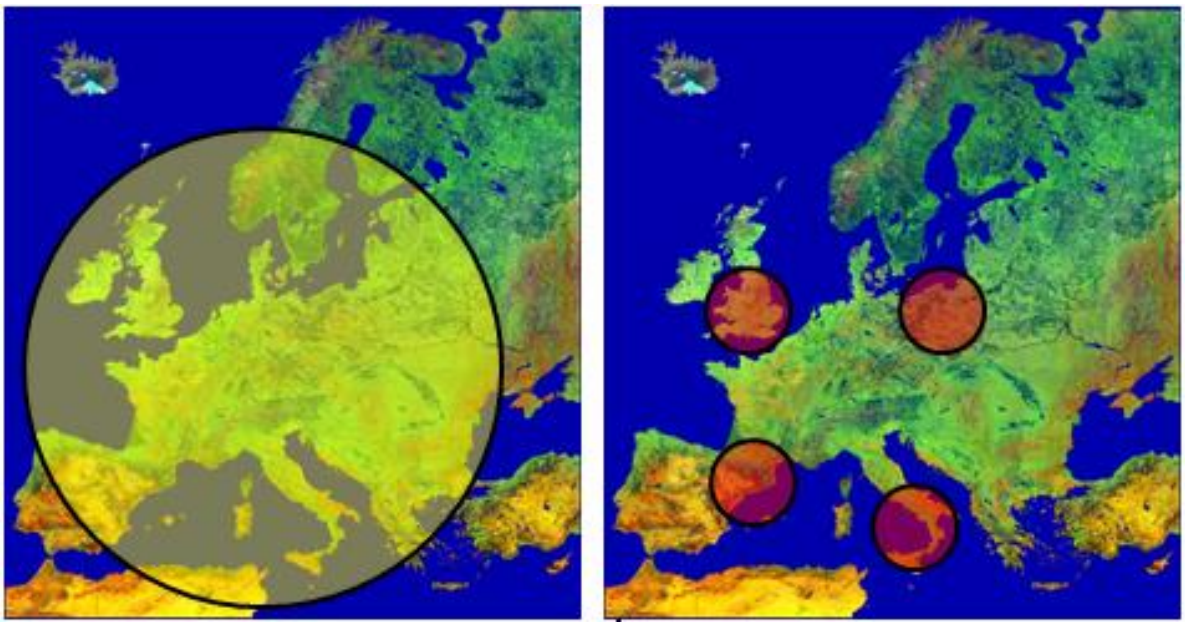

Figure 5: GEOSAR L-band beam coverage (left) and X-band beam coverage (right).

1.4. GEOSAR MISSION LIMITATIONS:

On the previous sections we talked about the advantages and capabilities of the GEOSAR missions, but these will also present some difficulties and limitations.

GEOSAR missions will place a radar payload in a satellite platform of a geostationary orbit. The radar payload will consequently be far away from the Earth's surface receiving a low power echo from the targets and resulting in a low Signal-to-Noise Ratio (SNR). The fact of using larger antennas or increasing the transmitted power is a possible first option in order to increase the SNR; however, this fact would suppose higher development and exploitation costs. There is a possible second option: SNR can be increased using along-track oversampling with a PRF (Pulse Repetition Frequency) well above the Doppler bandwidth, and operating the radar with a long integration time.

The integration time should be large (up to hours) in order to obtain medium resolution images (10 to 20 meters) using an X-band radar. Thus, the illumination energy can substantially increase. During this "large" integration time, the atmosphere could change and that could decorrelate the radar signals significantly. Note that in the LEOSAR missions the effect of the atmosphere can be considered invariant due to the fact that the integration time is small (1 second approximately). So, in order to avoid image defocusing, the temporal evolution of the atmosphere must be compensated before doing the azimuth SAR compression. This atmosphere retrieval will be performed by means of the atmospheric phase screen maps obtained for example by using the L-band radar (Ruiz Rodon et al., 2013).

Several sources affect the along-track phase history in GEOSAR missions causing undesired fluctuations which will cause image defocusing. These will be:

- Atmospheric Phase Screen (APS).
- Radar Carrier Frequency Drifts.
- Satellite altitude instabilities and structural vibration.
- Orbit determination errors.

Note that the main purpose of this project is to obtain simulated images of a GEOSAR mission. In order to obtain accurate images of the scene after SAR processing, the range history of every point of the scene is needed. So we need a high precision orbit model and suitable techniques to compensate the APS.

2. SATELLITE ORBITS

In physics, an orbit is the gravitationally curved path of an object around a point in space, for example the orbit of a planet around a star. Normally, the term orbit refers to a regularly repeating path around a body, although it may occasionally be used for a non-recurring trajectory or a path around a point in space. To a close approximation, planets and satellites follow elliptical orbits, with the central mass being orbited at a focal point of the ellipse, as described by Kepler's law of planetary motion.

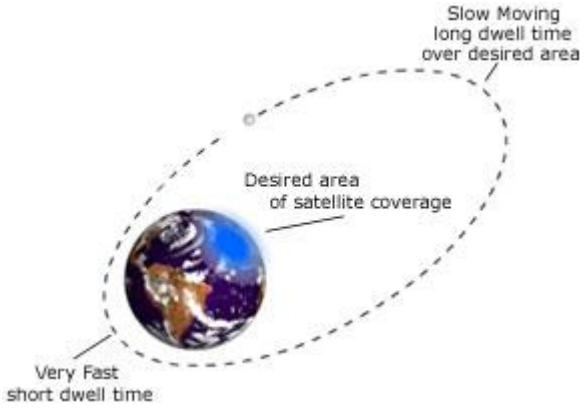

Figure 6: Elliptical Orbit Trajectory of a Satellite around the Earth.

2.1. HISTORY OF ORBITS

Historically, the concept of celestial sphere was used by philosophers to describe the apparent movement of planets. This concept describes the existence of perfect moving spheres in which the planets and the stars were attached. Note that this model was developed without any knowledge about the gravity force and it assumes that the heavens were fixed and not attached to any sphere. After the planet motions were more accurately measured, theoretical mechanisms such as deferent and epicycles were added. But this model has a problem, which is the precision. In order to predict accurately orbits, lots of epicycles were needed, so it became increasingly unwieldy. Copernicus simplify the model by placing the sun on the centre. It is the origin of the geocentric model.

Johannes Kepler formulate the basis of the modern understanding of orbits. The results Kepler found are summarised in what is known as the three laws of planetary motion. First, he prove that the orbits of the planets in the Solar System are not circular, they are elliptical and the Sun is not placed at the centre of this orbits, but rather on one focus. Second, he found that the planet's orbital speed is not a constant, it depends on how far the planet is from the Sun. Finally, Kepler found a universal relationship between the orbit properties of all the planets orbiting the Sun. For the planets, the cubes of their distances from the Sun are proportional to the squares of their orbital periods.

Isaac Newton demonstrate the validity of the Kepler law's from the fact that they were derivable from his theory of gravitation and that, in general, the orbits of bodies are subject to gravity generating conic sections. Newton showed that, for a pair of bodies, the orbit's sizes are in inverse proportion to their masses, and that those bodies' orbits share a common centre of mass. Note that when on body is much larger and heavier than the other one, it is convenient to approximate the centre of mass as coinciding with the centre of the bigger body.

Albert Einstein in his 1916 paper "*The Foundation of the General Theory of Relativity*" explained that gravity was produced by the curvature of space-time and removed Newton's assumption that changes propagate instantaneously. Then the Newtonian mechanics did not provide the highest accuracy in order to understand orbits. In the relativity theory, geodesic trajectories that can be extremely well approximated using Newtonian predictions (except in the presence of very strong gravity fields or very high speeds) are used to predict orbits.

2.2. KEPLER'S LAWS:

The orbital period is the time in which the bodies following closed orbits repeat their paths [21]. The laws of Kepler describe this motion, which can be derived from Newton's laws.

These can be formulated as follows:

1. The orbit of a planet around the Sun is an ellipse, with the Sun in one of the focal points of that ellipse. This focal point is actually the barycentre of the Sun-planet system; for the sake of simplicity this assumes that the Sun's mass is infinitely greater that the one of the planet. The orbital plane, is a plane in which the planet's orbit lies. The point on the orbit closest to the attracting body is the periapsis. The point farthest from the attracting body is called the apoapsis.

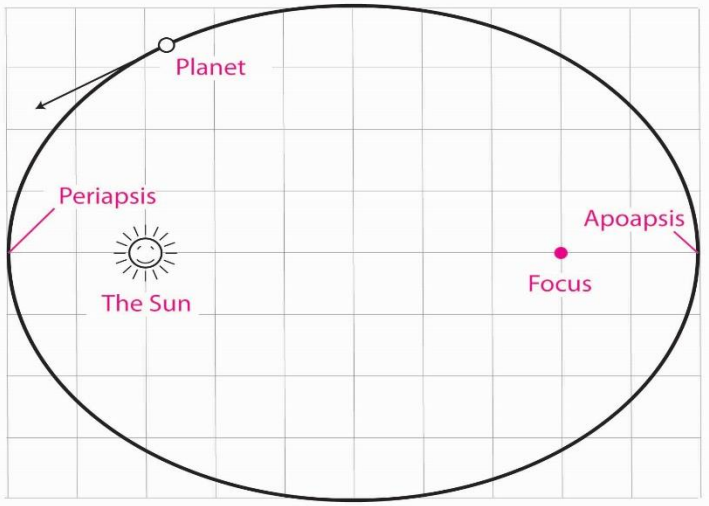

Figure 7: 1st Law of Kepler.

2. As the planet moves in its orbit, the segment from the Sun to planet weeps a constant area of the orbital plane for a constant period of time, regardless of which part of its orbit the planet traces during that period of time. This means that the planet moves faster near its perihelion than near its aphelion, because at the

smaller distance from the Sun it needs to move a greater segment of the orbit to cover the same area. This law is usually stated as “equal areas in equal time”.

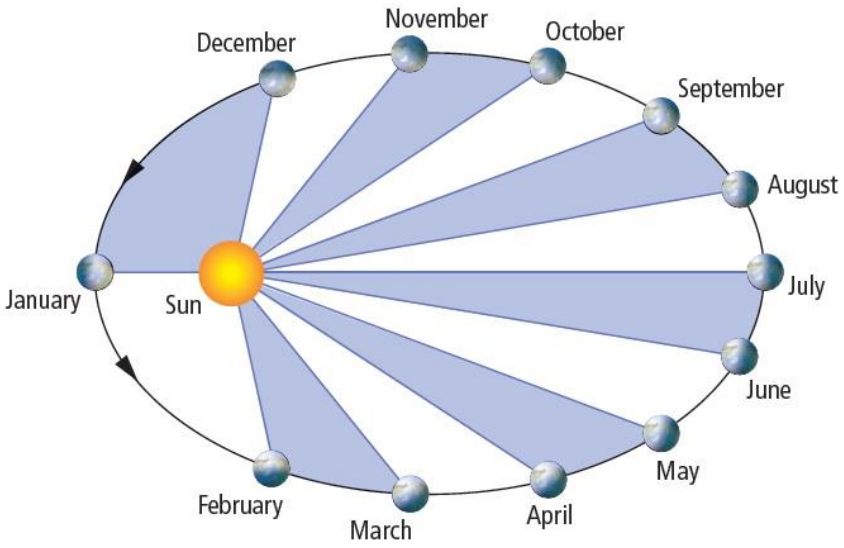

Figure 8: 2nd Kepler Law.

3. For a given orbit, the ratio of the cube of its semi-major axis to the square of its period is constant. After applying Newton’s Laws of Motion and Newton’s Law of Gravity we find that Kepler’s Third Law takes a more general form:

$$T^2 = \frac{4\pi^2 \cdot a^3}{G(M_1 + M_2)} \qquad (2.1)$$

Where M_1 and M_2 are the masses of the two orbiting objects in solar masses.

2.3. SPECIFYING ORBITS:

In order to specify a Keplerian orbit just six parameters are required. For example, the three numbers that specify the body’s initial position, and the three values that specify its velocity will define a unique orbit that can be calculated forwards (or backwards) in time. However, traditionally the parameters used are slightly different.

The set of Keplerian elements is traditionally used in order to specify an orbit.The Keplerian elements are six:

- Inclination (I): measures the tilt of an object's orbit around a celestial body. It is expressed as the angle between a reference plane and the orbital plane or axis of direction of the orbiting object.
- Longitude of the ascending node (Ω): angle from a reference direction, called the origin of longitude, to the direction of the ascending node, measured in a reference plane.
- Argument of periapsis (ω): angle from the body's ascending node to its periapsis, measured in the direction of motion.
- Eccentricity (e): parameter that determines the amount by which an orbit around a body deviates from a perfect circle.
- Semi major axis (a): is one half of the major axis, and thus runs from the centre, through a focus, and to the perimeter.
- Mean anomaly at epoch (M_0): angular distance from the pericenter which a fictitious body would have if it moved in a circular orbit, with constant speed, in the same orbital period as the actual body in its elliptical orbit.

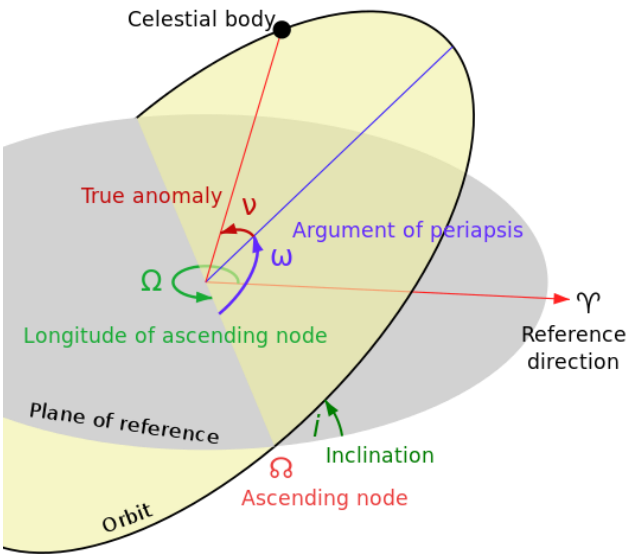

Figure 9: Diagram of orbital elements.

2.4. EARTH ORBITS:

2.4.1. LOW EARTH ORBIT (LEO):

A LEO orbit is an orbit around Earth with an altitude between 160 kilometres (orbital period of about 88 minutes) and 2000 km (about 127 minutes).

Objects in LEO encounter atmospheric drag from gases in the thermosphere or exosphere, depending on orbit height. Due to the atmospheric drag, satellites do not usually orbit below 300 km. Objects in LEO orbit Earth between the denser part of the atmosphere and below the inner Van Allen Radiation belt.

A LEO orbit is simplest and cheapest for satellite placement. It provides high bandwidth and low communication time lag (latency) , but satellites in LEO will not be visible from any given point on the Earth at all times.

2.4.2. MEDIUM EARTH ORBIT (MEO):

Sometimes called Intermediate Circular Orbit (ICO), is the region of space around the Earth above Low Earth Orbit (altitude of 2000 km) and below geostationary orbit (altitude of 35786 kilometres).

The most common use for satellites in this region is for navigation, communication and geodetic/space environment science. The most common altitude is approximately 20200 kilometres, which yields and orbital period of 12 hours, as used, for example, by the Global Positioning System (GPS).

2.4.3. GEOSYNCHRONOUS ORBIT (GSO):

A GSO is an orbit about the Earth of a satellite with an orbital period that matches the rotation of the Earth on its axis (one sidereal day) of approximately 23 hours 56 minutes and 4 seconds. The synchronization of rotation and orbital period means that, for an observer on the surface of the Earth, an object in geosynchronous orbit returns to exactly the same position in the sky after a period of one sidereal day.

2.4.4. GEOSTATIONARY ORBIT (GEO):

GEO are a special case of geosynchronous orbit. Is a circular geosynchronous orbit at zero inclination (that is, directly above the equator). They are also called geosynchronous equatorial orbits. Note that the altitude of the body in order to be in a GEO orbit should be 35786 kilometers.

2.4.5. HIGH EARTH ORBIT (HEO):

HEO is a geocentric orbit with an altitude entirely above that of a geosynchronous orbit. The orbital periods of such orbits are greater than twenty-four hours, therefore satellites in such orbits have an apparent retrograde motion, their orbital velocity is lower than Earth's rotational speed, causing their ground track to move westward on Earth's surface.

2.4.6. POLAR ORBIT:

Polar-orbiting satellites provide a more global view of Earth, circling at near-polar inclination (the angle between the equatorial plane and the satellite orbital plane is approximately 90 degrees). Orbiting at an altitude of 700 to 800 km, these satellites cover best the parts of the world more difficult to cover in situ.

These satellites operate in a sun-synchronous orbit. The satellite passes the equator and each latitude at the same local solar time each day, meaning the satellite passes overhead at essentially the same solar time throughout all seasons of the year.

2.4.7. ECCENTRIC/INCLINED ORBIT:

Eccentric/Inclined orbits have an inclination between 0 degrees (equatorial orbit) and 90 degrees (polar orbit). These orbits may be determined by the region on Earth that is of most interest or by the latitude of the launch side. The orbital altitude of these satellites is generally on the order of a few hundreds of kilometres, so the orbit period is on the order of a few hours. These satellites are not sun-synchronous.

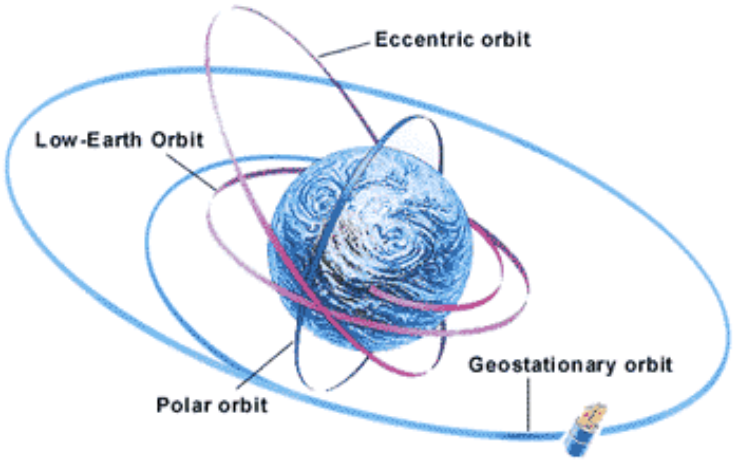

Figure 10: Different types of orbits around the Earth.

2.5. ORBITAL PERTURBATIONS:

Many factors should be considered when a satellite needs to be launched into the desired orbit. The orbit of the satellite should be maintained with a high precision in order to not collapse with other orbits of other active satellites. For example, a GEO satellite, which appears to be fixed in the sky, must maintain its longitude and latitude position such that it does not leave its desired position by more than ±0.05 degrees in the East-West direction and ±0.05 degrees in the North-South direction. At the altitude of a GEO satellite, this corresponds to a square in space that is roughly 70 km in each side.

Keeping a satellite in that square in the sky appears to be an easy task as this square is huge. However, in practice this is not true because of many factors [22]. Some of these factors include:

1. The weightlessness of objects in space makes them subject to the slightest forces acting on them. This means that when you are weightless, even a small force that acts on you in a specific direction will result in a huge acceleration in that direction. Over days, months, or even years, the accumulations of these accelerations become significant, and can move the satellite out of the target location.

2. The Keplerian model for the orbit of satellites is only true if we assume Earth as a point mass at the centre of its gravity. Clearly, this is not true because:

    a) Earth is not a perfect sphere but is flatter at the two poles than at the equator. The Earth's diameter over the equator is greater than the diameter that passing over the two poles by approximately 20 km.

    b) The radius of the Earth as you move over the equator changes.

    c) The density of Earth is not uniform but has higher values at specific regions causing a non-uniform gravitational force as a satellite moves in its orbit.

3. The gravity of the Sun and Moon which act on the satellite in different directions as their positions with respect to the satellite change over the time of the day, month and year.

4. Solar Winds: the Sun has been found to have periodic flares on the order of 11 years or so. Normally, the Sun emits relatively small amounts of solar winds. However, during these flares, huge amounts of solar winds are emitted to the point that satellite communications are often interrupted during these solar flares. These solar winds are charged particles that travel at high speeds away from the Sun. These particles act on satellites causing them to move.

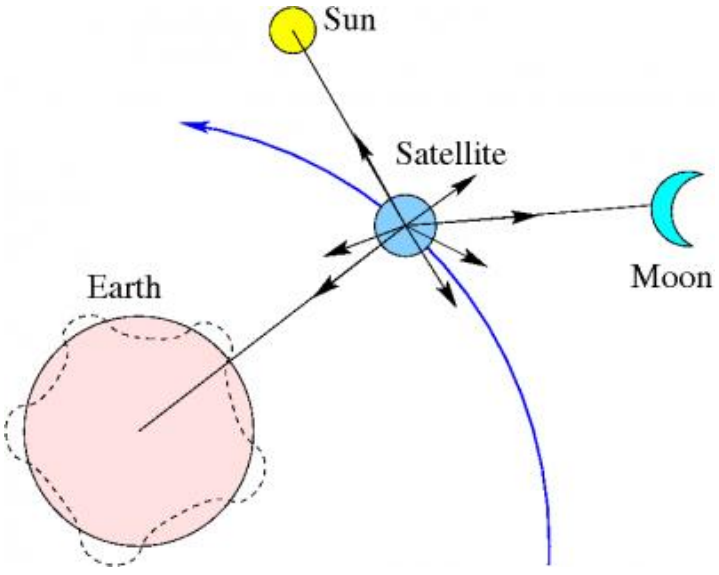

Figure 11: Effect of the gravity of the Sun and the Moon over a satellite.

3. SYNTHETIC APERTURE RADAR (SAR)

Synthetic Aperture Radar (SAR) is a form of radar that is used to create two- or 3-dimensional images of the Earth surface [1] [2] [3] [4] [5] [17]. SAR uses the motion of the radar antenna over a target region to provide finer spatial resolution than conventional beam-scanning radars. SAR is typically mounted on a moving platform such as an aircraft or spacecraft, and has its origin in an advanced form of side-looking airborne radar (SLAR).

The larger the aperture, the higher the image resolution will be, regardless of whether the aperture is physical (a large antenna) or "synthetic" (a moving antenna) – this allows SAR to create high resolution images (on the order of 1 meter to 10 meters) in comparation with small physical antennas.

To create a SAR image, successive pulses of radio waves are transmitted to "illuminate" a target scene, and the echo of each pulse is received and recorded. The pulses are transmitted and the echoes received using a single beam-forming antenna, with wavelengths of a meter down to several millimetres. As the SAR device on board the aircraft or spacecraft moves, the antenna location relative to the target changes with time. Signal processing of the successive recorded radar echoes allows the combining from these multiple antenna positions – this process forms the 'synthetic antenna aperture', and allows the creation of higher resolution images than would otherwise be possible with a given physical antenna.

Figure 12: Strip map Synthetic Aperture Radar (SAR) of Washington DC.

3.1. GEOSYNCHRONOUS SAR ACQUISITION PARAMETERS:

The most important parameters of SAR acquisition will be explained for a general GEOSAR acquisition, taking in count a low-inclined low-eccentricity orbit. This section is based on Ruiz Rodon's "Study on the feasibility of geosynchronous satellites for synthetic aperture radar applications" [4] and all the figures are extracted from it.

3.1.1. SPHERE'S GEOMETRY BASIS:

For understanding the relation between the different parameters that define a GEOSAR system we will need to understand the basic aspects of spherical trigonometry.

The spherical geometry is the study of the geometry of the surface of a sphere.

A great circle is defined by the intersection of the sphere with a plane which contains the centre of the sphere. Small circles are generated by all the other intersections that do not contain the centre of the sphere.

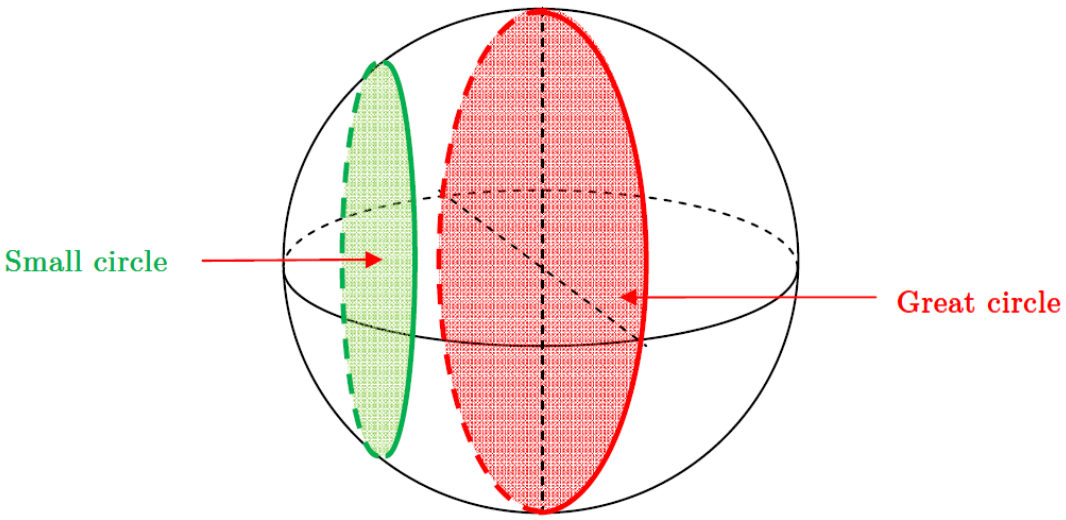

Figure 13: Geometry of the sphere (great circle and small circle definition). Source: [4]

A spherical triangle is a triangle drawn on the surface of a sphere whose sides are all arcs of great circles. Moreover, a spherical triangle has to accomplish three additional properties:

1. The addition of two sides is always greater than the remaining one.
2. The addition of the three angles is greater than 180°.
3. Each individual spherical angle is less than 180°.

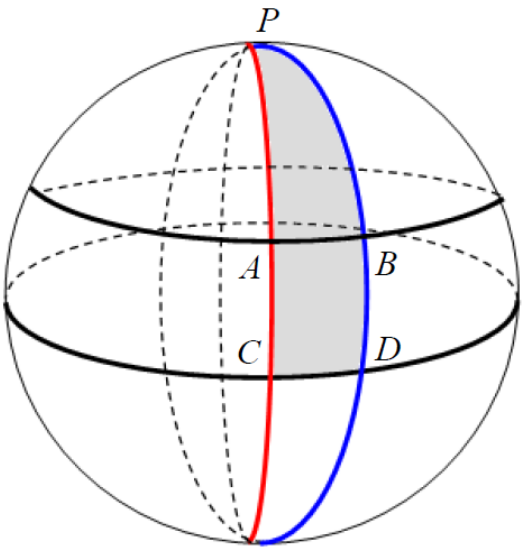

Figure 14: Spherical triangles over a sphere surface. Source: [4]

3.1.2. GEOSYNCHRONOUS SATELLITE TRACK:

The satellite track is defined as the group of points in the intersection of the Earth's center-satellite vector with the surface of the Earth. In order to obtain the satellite track, the satellite motion respectively to the center of the rotating Earth should be used.

In the next figure (Figure 15) a fixed Earth scheme is presented. The coordinates of the satellite $(\lambda'_{SL}, \varphi_{SL})$ define the longitude and latitude at a given time with respect to a reference meridian and to the equator, respectively. The longitude of the ascending node with respect to the reference meridian is called λ_{AN} and it will be used to relate the longitudinal and latitudinal coordinates of the satellite.

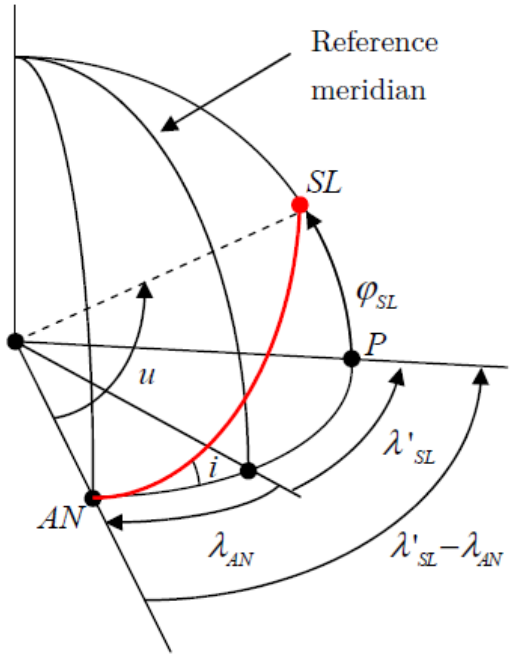

Figure 15: Satellite track for fixed Earth reference system. Source: [4]

$$\cos(\lambda'_{SL} - \lambda_{AN}) \cos 90^{\circ} = \sin(\lambda'_{SL} - \lambda_{AN}) \cos \varphi_{SL} - \sin 90^{\circ} \cot i$$

$$0 = \sin(\lambda'_{SL} - \lambda_{AN}) \cos \varphi_{SL} - \cot i$$

$$\frac{1}{\tan i} = \sin(\lambda'_{SL} - \lambda_{AN}) \frac{1}{\tan \varphi_{SL}}$$

$$\tan \varphi_{SL} = \sin(\lambda'_{SL} - \lambda_{AN}) \tan i \qquad (3.1)$$

The formula 3.1 relates some important parameters such as the satellite latitude, longitude, the orbit inclination and the longitude of the ascending node.

However, the Earth is not fixed, it rotates so we need a rotational Earth reference system. To do that, it is important to take into account a rotation of the reference meridian along time. The time elapsed from the satellite pass through the reference meridian is expressed as Δt. The reference time is usually taken on the satellite cross through the perigee, so Δt can be written as $\Delta t = t_p - t_0$, where t_p is the time elapsed since the

satellite reach the perigee and $t_0$is the time of the initial position of the reference meridian computed from the passage through the perigee.

Then, the changes of the reference meridian position due to the Earth rotation (Ω_E) can be expressed as $\Delta\lambda = \Omega_E(t_p - t_0)$. This will produce a change on the relative longitude (λ_{SL}) of the satellite with respect this Earth rotating reference system. Finally, the satellite longitude with respect to the new rotational Earth reference system can be expressed as $\lambda_{SL} = \lambda'_{SL} - \Delta\lambda$.

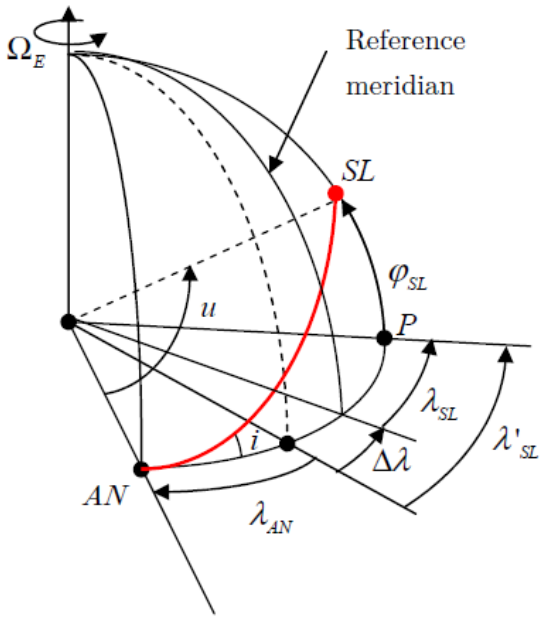

Figure 16: Satellite track in a rotating Earth reference system. Source: [4]

3.1.2.1 LONGITUDE HISTORY OF THE SATELLITE TRACK:

In order to make things easy, we can consider as the reference meridian the one crossing at the longitude of the ascending node. This is equivalent to consider the longitude of the ascending node (λ_{AN}) equal to zero. Considering that, note that:

$$\sin\lambda'_{SL} = \frac{\tan\varphi_{SL}}{\tan i} \quad (3.2)$$

$$\cos\lambda'_{SL} = \frac{\cos u}{\cos\varphi_{SL}} \quad (3.3)$$

$$\tan \lambda'_{SL} = \tan u \cos i \quad (3.4)$$

Considering a rotational reference system, the longitude of the satellite respectively to the meridian of the ascending node, can be obtained in some different ways as follows:

$$\lambda_{SL} = \lambda'_{SL} - \Delta\lambda = \sin^{-1}\left(\frac{\tan \varphi_{SL}}{\tan i}\right) - \Delta\lambda \quad (3.5)$$

$$\lambda_{SL} = \lambda'_{SL} - \Delta\lambda = \cos^{-1}\left(\frac{\cos u}{\cos \varphi_{SL}}\right) - \Delta\lambda \quad (3.6)$$

$$\lambda_{SL} = \lambda'_{SL} - \Delta\lambda = \tan^{-1}(\tan u \cos i\ ) - \Delta\lambda \quad (3.7)$$

On the other hand, considering the mean anomalies of the satellite and the ascending node, the term Δλ can be re-written. The mean anomaly (M) is defined as the true anomaly of an equivalent satellite in a circular orbit of the same period. The mean anomaly can be obtained as a function of time with respect to the time of passage through the perigee:

$$M = \frac{2\pi}{T}(t - t_p) = n(t - t_p) \quad (3.8)$$

Being *n* the mean angular velocity or mean movement of the satellite with period T. Then:

$$\Delta\lambda = \Omega_E(t_p - t_0) = \Omega_E\left(\frac{M_S}{n} - \frac{M_0}{n}\right) = \frac{\Omega_E}{n}(M_S - M_0) \quad (3.9)$$

If a geosynchronous satellite period is the same as the one of the rotation of the Earth, the mean movement (n) equals Ω_E. The angle between the ascending node and the position of the satellite, known as u, can be calculated as the addition of the true anomaly of the satellite (υ) and the argument of the perigee (ω). Another important parameter that usually appears on the orbital analysis is the eccentric anomaly (E). The eccentric anomaly corresponds to the true anomaly of the satellite at the present time mapped to an equivalent circular orbit. The relationship between the mean anomaly and the eccentric anomaly is:

$$M = E - e \sin E \quad (3.10)$$

With the previous considerations and the equations (3.9) and (3.10), the longitude of the satellite can be finally obtained as:

$$\lambda_{SL} = \tan^{-1}(\tan(\omega + v)\cos i) - (E - e\sin E) + (E_0 - e\sin E_0) \quad (3.11)$$

For quasi-circular ($e \approx 0$) and non-inclined ($e < 1°$) orbits, the satellite relative longitude with respect the nominal satellite can be approximately expressed as:

$$\lambda_{SL} = \lambda_{SL_0} + 2e\sin\left(\Omega_E(t_p - t_0)\right) \quad (3.12)$$

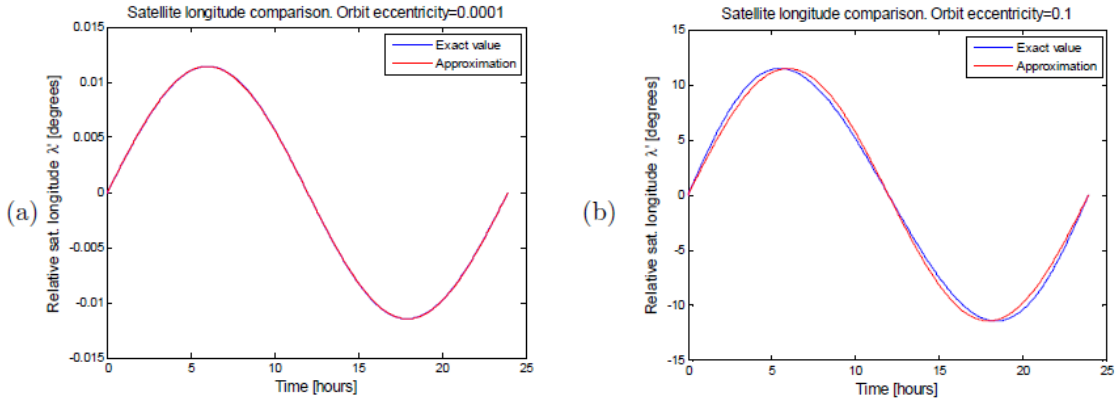

Figure 17: Satellite relative longitude evolution approximation. a) Considering an orbit eccentricity of 0.00001 and b) 0.1. Source: [4]

3.1.2.2 LATITUDE HISTORY OF THE SATELLITE TRACK:

Earth rotation does not affect to the latitude and consequently, the latitude does not depend on the origin position or reference meridian choice, differently that in the longitude case. The satellite latitude can be expressed as:

$$\varphi_{SL} = \sin^{-1}(\sin i \sin u) = \sin^{-1}(\sin i \sin(\omega + v)) \quad (3.13)$$

The arcsine function can be approximated by its argument while the $\sin i \approx i$ considering the geosynchronous case with a slightly inclined orbit. Therefore, the satellite latitude can be approximately expressed as:

$$\varphi_{SL} = i \sin\left(\omega + \Omega_E\left(t - t_p\right)\right) \qquad (3.14)$$

Where the reference time has been taken the time across the perigee similarly to the longitude case. Therefore, elliptical tracks will be typically obtained combining the longitudinal and latitudinal motions given by (3.12) and (3.14). Therefore, the longitudinal displacements of the satellite respectively to its nominal longitude will be governed by the eccentricity. On the other hand, the satellite latitudinal motion respectively to the equatorial plane will be determined by the inclination. Finally the angular shift between the two components will be established by the argument of the perigee, resulting in linear, elliptical or quasi-circular shapes of the relative satellite-motion.

3.1.3. SATELLITE-TARGETS SLANT RANGE:

The distance to the targets that the satellite illuminates is one of the most important parameters of the remote sensing systems. It will be important to recognize the source of the received echoes as well as in the computation of the power link budget. The distance from the satellite to a target located at coordinates (λ_T, φ_T) over the Earth will depend on the satellite coordinates $(\lambda_{SL}, \varphi_{SL})$ and the geographical height (h_T) of the point over the Earth reference ellipsoid.

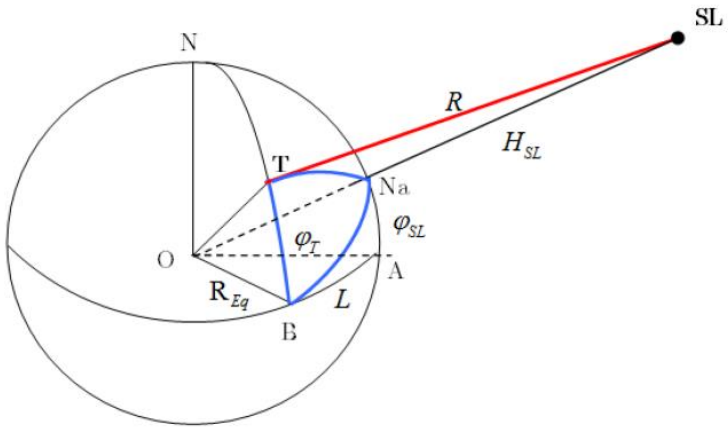

Figure 18: Earth-Satellite Geometry. Source: [4]

The satellite latitude in Figure 18 is given by the angle NaOA, where Na is the sub-satellite point (or nadir) and the angle TOB corresponds to the target latitude. The relative longitude between the satellite and the target is another important parameter that should be taken into account in the distance computation. This angle, called $L = \lambda_T - \lambda_{SL}$ is defined by AOB.

Range which is the term used in radar for the distance between the satellite and the target is computed using the triangle OTSL. The side $\overline{OT}$ which corresponds to the location of the target over the Earth's surface can be obtained as the result of the local Earth's radius at that latitude adding to that the ellipsoidal height (h_T) of the desired target. The side $\overline{OSL}$ corresponds to distance of the satellite to the Earth's centre and can be easily obtained from the orbit analysis of the geosynchronous case with the two body problem and corresponds to the addition of the local Earth's radius at the nadir point plus the satellite height over the nadir. Finally, the side $\overline{TSL}$ is the goal which corresponds to the distance between the satellite and the desired target usually known as range.

Note that using an ellipsoidal reference model we will obtain more precise results.

Using the linear cosine law over the OTSL triangle, the range, which again is the distance between the satellite and the target can be computed. Then, the following equation is obtained:

$$R_{SL-T} = \sqrt{(R_{ET} + h_T)^2 + r^2 - 2(R_{ET} + h_T) r \cos\phi} \qquad (3.15)$$

Where R_{ET} is the local Earth's radius at the target latitude, h_T is the target height over the reference ellipsoid, r is the orbital radius of the satellite and ϕ is the angle TONa. From the spherical triangle NaTB we can obtain the angle ϕ. Note that the triangle mentioned is remarked in blue in the previous figure (figure 18).

$$\cos\phi = \cos\varphi_T \cos\xi + \sin\varphi_T \sin\xi \cos TBNa \qquad (3.16)$$

Applying the sine and cosine spherical laws over the BANa triangle we can obtain the $\sin\xi$ and $\cos\xi$. On the other hand, $\widehat{TBNa} = \pi/2 - i$ and, therefore, $\cos\widehat{TBNa} = \cos(\pi/2 - i) = \sin i$. Then we can obtained another expression for $\cos\phi$:

$$\frac{\sin\widehat{NaAB}}{\sin\xi} = \frac{\sin i}{\sin\varphi_{SL}} \rightarrow \sin\xi = \frac{\sin 90^{\circ}\sin\varphi_{SL}}{\sin i} = \frac{\sin\varphi_{SL}}{\sin i} \qquad (3.17)$$

$$\cos\xi = \cos\varphi_{SL}\cos L + \sin\varphi_{SL}\sin L\cos\widehat{NaAB} = \cos\varphi_{SL}\cos L + \sin\varphi_{SL}\sin L\cos 90^{\circ}$$
$$= \cos\varphi_{SL}\cos L \qquad (3.18)$$

$$\cos\phi = \cos\varphi_T\cos\varphi_{SL}\cos L + \sin\varphi_T\frac{\sin\varphi_{SL}}{\sin i}\sin i = \cos\varphi_T\cos\varphi_{SL}\cos L + \sin\varphi_T\sin\varphi_{SL} \qquad (3.19)$$

Using this result in (3.15), the target-satellite range can be computed as:

$$R_{SL-T} = \sqrt{(R_{ET}+h_T)^2 + r^2 - 2(R_{ET}+h_T)r(\cos\varphi_T\cos\varphi_{SL}\cos L + \sin\varphi_T\sin\varphi_{SL})} \qquad (3.20)$$

The slant range will change along the orbit accordingly to the satellite coordinates evolution get from (3.12) and (3.14) in the particular case of the GEOSAR with slight satellite longitude and latitude variations caused by small eccentricities and inclinations considered in this analysis. Besides, variations on the orbit radius r will be produced by the small eccentricity, which will increase the fluctuations in the satellite-target distance. The parameters referred to the point $(\varphi_T, \lambda_T, h_T)$ are fixed if a still point over the Earth's surface is considered.

3.1.4. SATELLITE LOCATION: ELEVATION AND AZIMUTH ANGLES:

From a point of view of a target located at the Earth surface, the satellite is seen on the sky in a fixed zone with slightly variations due to the relative motion of the non-prefect geostationary orbit of the satellite. Two angles are needed in order to define the location of the satellite and the generally used are the elevation and azimuth angles. Normally, the satellite motion in the sky is called analemma of the satellite.

3.1.4.1 ELEVATION ANGLE:

The elevation angle is defined as the angle between the horizon at the point where the target is placed and the direction of the satellite measured in the plane that contains the satellite, the center of the Earth and the considered target. The elevation angle, called θ_{el}^{T}, can be computed using the triangle O-T'-SL shown in the figure.

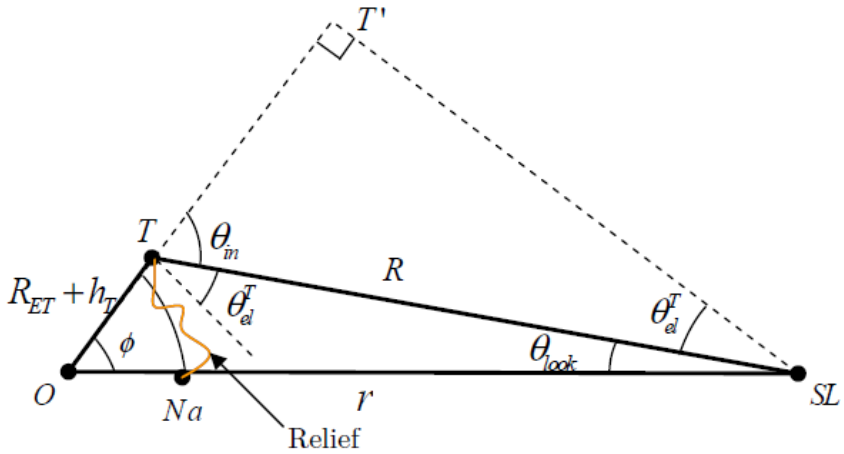

Figure 19: Satellite Location in the sky. Elevation angle computation. Source: [4]

The angle T'TSL in the figure is equal to $\pi/2 - \theta_{el}^{T}$. Since the angles of the triangle T-T'-SL should be equal to π radians, the angle $T'TSL = \pi - (\pi/2 - \theta_{el}^{T}) - \pi/2 = \theta_{el}^{T}$. Then, using planar trigonometry, the elevation angle can be calculated as:

$$\cos \theta_{el}^{T} = \frac{\overline{T'SL}}{R} \qquad (3.21)$$

Where the segment $\overline{T'SL}$ can be obtained from the triangle O-T'-SL as:

$$\sin\phi = \frac{\overline{T'SL}}{r} \qquad (3.22)$$

Therefore, the elevation angle is computed in the next equation:

$$\theta_{el}^{T} = \cos^{-1}\left(\sin\phi\frac{r}{R}\right) \qquad (3.23)$$

Similarly, the elevation angle can also be calculated considering the sine of the angle TSLT'. The analysis is presented next:

$$\sin\ \theta_{el}^{T} = \frac{\overline{\overline{T'T}}}{R} \qquad (3.24)$$

And

$$\cos\phi = \frac{(R_{ET} + h_T) + \overline{\overline{T'T}}}{r} \rightarrow \overline{T'T} = r\cos\phi - (R_{ET} + h_T) \qquad (3.25)$$

Using (3.24) and (3.25), another way to obtain the elevation angle is the following:

$$\theta_{el}^{T} = \sin^{-1}\left(\frac{\cos\phi - (R_{ET} + h_T)/r}{R/r}\right) \qquad (3.26)$$

Finally, taking the results of equations (3.23) and (3.26), the elevation angle is given in terms of the tangent as:

$$\tan\ \theta_{el}^{T} = \frac{\sin\ \theta_{el}^{T}}{\cos\ \theta_{el}^{T}} = \frac{\dfrac{\cos\phi - (R_{ET} + h_T)/r}{R/r}}{\sin\phi\dfrac{r}{R}} = \frac{\cos\phi - (R_{ET} + h_T)/r}{\sin\phi}$$

$$\theta_{el}^{T} = \tan^{-1}\left(\frac{\cos\phi - (R_{ET} + h_T)/r}{\sin\phi}\right) \qquad (3.27)$$

3.1.4.2 AZIMUTH ANGLE:

The azimuth angle is the other one needed in order to locate the satellite in the sky. This angle is measured in the incidence plane where the target is located between the direction of the geographic north and the direction to the satellite nadir point over the Earth's surface. It corresponds to the spherical angle NTNa in Figure 19. Depending on the orientation of the satellite with respect to the target consideredm the azimuth angle can take values from 0 to 360 degrees. If we apply the spherical law of sinus in the spherical triangle N-Na-T, we obtain:

$$\frac{\sin NTNa}{\sin(\pi/2 - \varphi_{SL})} = \frac{\sin NTNa}{\sin \phi} \qquad (3.28)$$

As it can be seen in Figure 19, the angle TNNa is equal to BNA. This angle can be obtained from the spherical triangle N-B-A as:

$$\frac{\sin BNA}{\sin L} = \frac{\sin BAN}{\sin BON} = 1 \qquad (3.29)$$

Since $BAN = BON = 90^{\circ}$, the angle NTNa which since now will be called a in order to make things easy, can be re-written as:

$$a = \sin^{-1}\left(\frac{\sin TNNa}{\sin \phi}\sin\left(\frac{\pi}{2} - \varphi_{SL}\right)\right) = \sin^{-1}\left(\frac{\sin L}{\sin \phi}\cos(\varphi_{SL})\right) \qquad (3.30)$$

The angle a computed with (3.30) always give an angle between 0 and 90 degrees. A transformation will be necessary to obtain the final value of the azimuth angle since the azimuth angle can be up to 360 degrees. Taking into account the relative position of the nadir point with respect to the target location after obtaining the angle a, the azimuth angle (θ_{az}^{T}) can be obtained.

Note that the position of the nadir point respectively to the target location has 4 possible solutions. All of them are represented in the next figure (Figure 20). The black dot represents the target location while the red one marks the sub-satellite point or nadir

position. Note that, the azimuth angle (θ_{az}^{T}) is computed in different ways (listed in the table below) from a, depending on the relative position of the nadir respect the target.

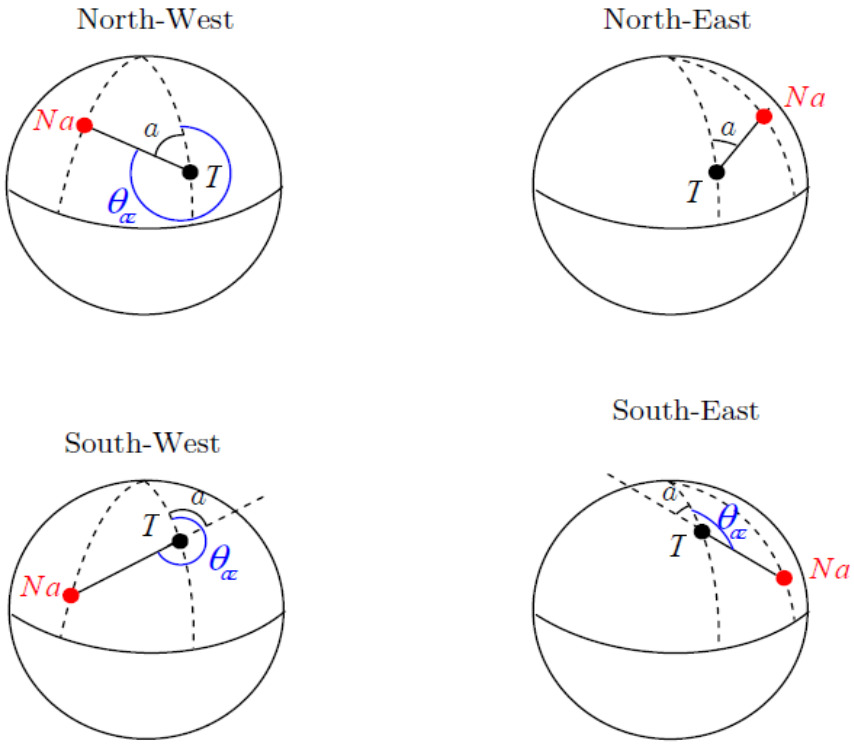

Figure 20: Determination of the azimuth angle. Source: [4]

Sub-satellite point (Na) with respect to the target (T)	Relation between θ_{az} and a (degrees)
North-West	$\theta_{az}^{T} = 360^{\circ} - a$
North-East	$\theta_{az}^{T} = a$
South-West	$\theta_{az}^{T} = 180^{\circ} + a$
South-East	$\theta_{az}^{T} = 180^{\circ} - a$

Table 4.1. Azimuth angle computation depending on the satellite-target position. [4]

3.1.5 TARGET LOCATION: LOOK AND INCIDENCE ANGLES:

The situation in the previous section can be equivalently seen from the point of view of the satellite. A target over a surface is seen from the satellite in a determined position. Using the look angle, the relative location of a target over the Earth surface can be determined from the point of view of the satellite.

3.1.5.1 LOOK ANGLE:

The look angle is defined as the angle between the nadir direction, perpendicular to the Earth's surface and the direction of the illuminated target. This angle, called θ_{look}, corresponds to the angle $\widehat{TSLO}$ in Figure 19. The nadir angle is another way of calling the look angle. Using the cosine law in the triangle T-SL-O:

$$(R_E + h_T)^2 = r^2 + R^2 - 2rR\cos\theta_{look} \qquad (3.31)$$

Then, the look angle can be computed as:

$$\theta_{look} = \cos^{-1}\left(\frac{r^2 + R^2 - (R_E + h_T)^2}{2rR}\right) \qquad (3.32)$$

Given the large distance between the satellite and the Earth the range of possible look angles will be really small in the geosynchronous case. When the incoming beam from the satellite is tangent to the surface of the Earth, we obtain the maximum look angle. It means that the angle between the incoming beam and the Earth's radius at this point is a right angle. Then using the law of sinus, we can easily obtain the maximum look angle:

$$\frac{\sin\theta_{look\_max}}{R_{pol} + h_T} = \frac{\sin 90^{\circ}}{r} \rightarrow \theta_{look\_max} = \sin^{-1}\left(\frac{R_{pol} + h_T}{r}\right) \qquad (3.33)$$

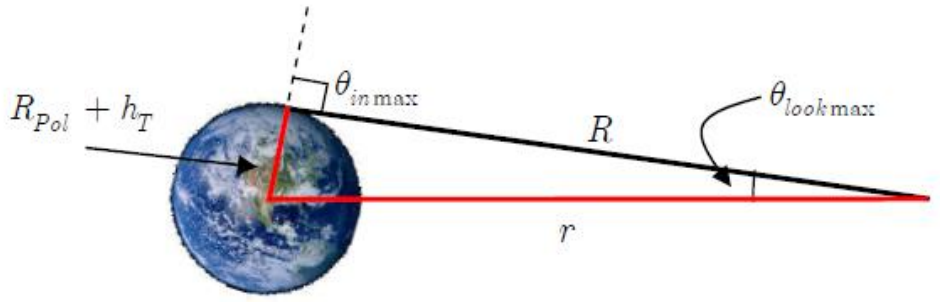

Figure 21: Maximum look angle. In the geosynchronous case, only a small range of look angles are allowed. Source: [4]

Note that high accuracy on the antenna pointing is needed because the look angle's critical parameter nature. Otherwise, small errors in pointing direction will result in large antenna footprint misalignment on the ground.

3.1.5.2 INCIDENCE ANGLE:

Incidence angle does not provide any different information as it is related with the look angle, but is widely used in most of the SAR and radar backscattering analysis.

The incidence angle is the angle between the direction of the incoming satellite illumination and the direction perpendicular to the incidence plane which is the plane tangent to the Earth's sphere at the target location. It corresponds to the angle $\widehat{T'TSL}$ in Figure 19, where it is marked as θ_{in}. The incidence angle can be obtained directly form the elevation angle as:

$$\theta_{in} = \frac{\pi}{2} - \theta_{el}^{T} \quad (3.34)$$

The slopes or local topography of the imaged scene are taken into account by the actual incidence angle. Using the law of sinus in triangle O-T-SL:

$$\frac{\sin\theta_{look}}{R_E + h_T} = \frac{\sin(\pi - \theta_{in})}{r} = \frac{\sin\theta_{in}}{r} \rightarrow \theta_{in} = \sin^{-1}\left(\sin\theta_{look}\frac{r}{R_E + h_T}\right) \quad (3.35)$$

In this case, the range of possible incidence angles for the geosynchronous case will vary from 0 degrees, corresponding to the nadir direction, to 90 degrees when the illumination is tangent to the Earth's surface.

$$\theta_{in\_max} = \sin^{-1}\left(\frac{R_{pol} + h_T}{r}\frac{r}{R_{pol} + h_T}\right) = \sin^{-1}(1) = 90^{\circ} \qquad (3.36)$$

3.2 GEOSYNCHRONOUS SAR COVERAGE:

The desired ground coverage or antenna footprint extension is another important parameter to take into account in the SAR design. This parameter is the ground patch that the radar is illuminating for a given look angle. The swath will depend on the look angle at which the antenna is pointing.

The large antenna coverage is one of the advantages of GEOSAR acquisition in front of current LEOSAR or GB-SAR. The field-of-view (FOV) of a single satellite will cover a large region of the Earth. An entire continent can be covered with a single GEOSAR satellite. However, due to the low gain of the antenna it would not be possible to cover different large areas simultaneously, resulting in high transmitted power requirements. So, a narrow beam should be considered and by changing the beam spotting we will be able to periodically illuminate the different zones accessible from the satellite.

An acquisition scheme like the one presented in the Figure 22 is the typical one. Note that the satellite's look angle is fixed, while the antenna beamwidth $\Delta\theta_{look}$ is the parameter determining the ground coverage of the system. Looking at the geometric parameters, the ground coverage (G_{cov}) can be calculated from the inner angles α_1 and α_2 as:

$$G_{cov} = \Delta\alpha \cdot R_{ET} = (\alpha_2 - \alpha_1) \cdot R_{ET} \qquad (3.37)$$

Where R_{ET} is the local Earth's radius in the illuminated area. Using the law of sinus we can easily obtain the inner angles α_1 and α_2:

$$\alpha_1 = \sin^{-1}\left(\sin\theta_{look\_near}\frac{R_{near}}{R_{ET}}\right) \quad (3.38)$$

$$\alpha_2 = \sin^{-1}\left(\sin\theta_{look\_far}\frac{R_{far}}{R_{ET}}\right) \quad (3.39)$$

Note that R_{near} stands for the range to the nearest target illuminated by the satellite. On the other hand, R_{far} corresponds to the furthest one. On the same way, θ_{look_near} and θ_{look_far} are the look angles at which the nearest and the furthest targets are observed. These angles can be easily calculated from the middle look angle and the beamwidth ($\Delta\theta_{look}$):

$$\theta_{look\_near} = \theta_{look} - \frac{\Delta\theta_{look}}{2} \quad (3.40)$$

$$\theta_{look\_far} = \theta_{look} + \frac{\Delta\theta_{look}}{2} \quad (3.41)$$

Finally, solving the second degree equation from the law of cosines the near and far slant range can be calculated. In those equations, r is the orbit radius while the look angles near and far corresponds to the ones computed in the previous equations (3.40) and (3.41). Finally, the ground coverage can be obtained from the look angle and the antenna beamwidth:

$$R_{near}^2 - 2r\cos\theta_{look\_near}R_{near} = R_{ET}^2 - r^2 \quad (3.42)$$

$$R_{far}^2 - 2r\cos\theta_{look\_far}R_{far} = R_{ET}^2 - r^2 \quad (3.43)$$

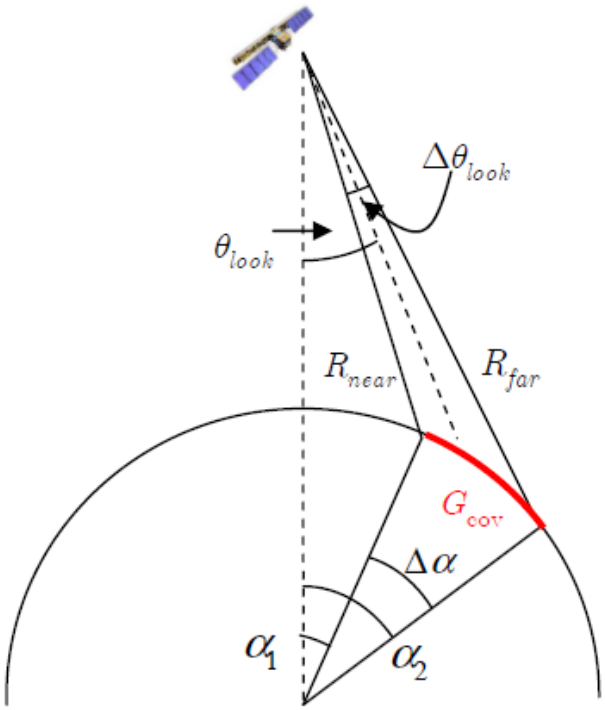

Figure 22: Ground coverage of the satellite. Source: [4]

In order to reach the desired coverage requirements of the GEOSAR systems, high antenna gains and very small beamwidths should be used.

Sometimes it can be useful to obtain the necessary antenna beamwidth to reach a desired swath width or coverage for a given look angle. The isolation of the antenna beamwidth is really complicated and it cannot be solved by linear algebra. So, in order to reach the desired beamwidth a reasonable approximation must be applied. Locally flat Earth is the most widely used approximation.

The ground coverage can be approximated as:

$$\overline{G_{cov}} = \frac{\Delta\theta_{look} R}{\cos\theta_{in}} \qquad (3.44)$$

Note that R is the slant range at the middle look angle and θ_{in} corresponds to the incidence angle obtained from (3.35). So, the necessary antenna beamwidth can be calculated from the desired swath as:

$$\Delta\theta_{look} = \frac{\overline{\overline{G_{cov}}\cos\theta_{in}}}{R} \qquad (3.58)$$

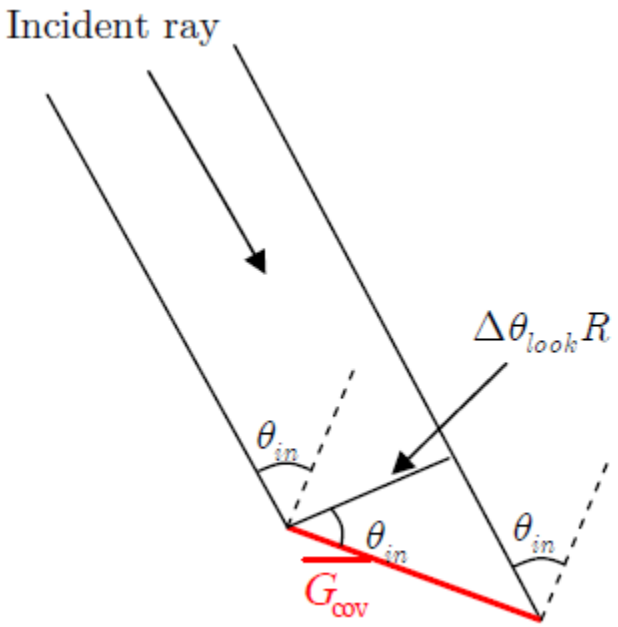

Figure 23: Flat surface approximation in swath ground coverage computation.
Source: [4]

3.3 BISTATIC SAR:

This project is focused on the bistatic GEOSAR with a receiver-on-ground antenna configuration. However, in this section the main aspects of the bistatic GEOSAR with a satellite-receiver antenna are explained for the sake of simplicity.

In the case of a bistatic SAR, some additional parameters must be defined. In Figure 24, the bistatic range cut is shown. In the bistatic acquisition, the parameters explained in the previous sections are still valid. Note that in the next figure, the subscripts T and R are used to identify the parameters corresponding to the transmitting and receiving paths,

respectively. In the bistatic case, the baseline vector from the transmitter to the receiver antenna phase centres and the transmitter-target-receiver angle, known as the bistatic angle complete the geometric parameters of the acquisition.

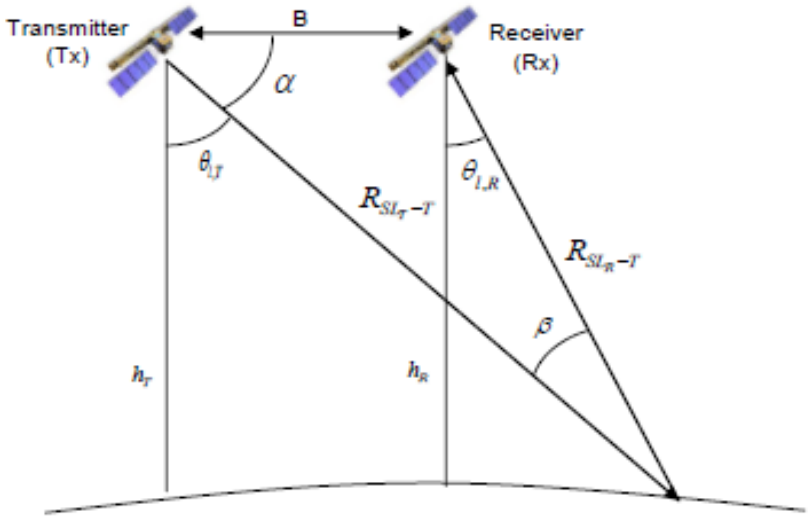

Figure 24: Bistatic SAR geometry in the bistatic plane. Source: [4]

Using the law of sines, the bistatic angle can be derived from the baseline B and the remaining geometric parameters as:

$$\beta = \sin^{-1}\left(\frac{B}{R_{SL_R-T}}\sin\alpha\right) \qquad (3.59)$$

Where,

$$\alpha = \cos^{-1}\left(\frac{B}{2(R_{ET}+h_T)}\right) - \theta_{l,T} \qquad (3.60)$$

$$R_{SL_T-T} = (R_{ET}+h_T)\cos\theta_{l,T} - \sqrt{R_{ET}^2 - (R_{ET}+H)^2 sin^2\theta_{l,T}} \qquad (3.61)$$

$$R_{SL_R-T} = \sqrt{{R_{SL_T-T}}^2 + B^2 + 2R_{SL_T-T}B\cos\alpha} \qquad (3.62)$$

4. COORDINATES SYSTEMS:

4.1. EARTH-CENTERED EARTH-FIXED (ECEF):

The Cartesian coordinate frame of reference used in GPS/GLONASS is called Earth-Centered, Earth-Fixed (ECEF). ECEF uses a three-dimensional XYZ coordinates (in meters) to describe the location of a target or satellite. The term "Earth-Centered" comes from the fact that the origin of the axis (0, 0, 0) is located at the mass centre of gravity (determined through years of tracking satellite trajectories). The term "Earth-Fixed" implies that the axes are fixed with respect to the Earth (that is, they rotate with the Earth).

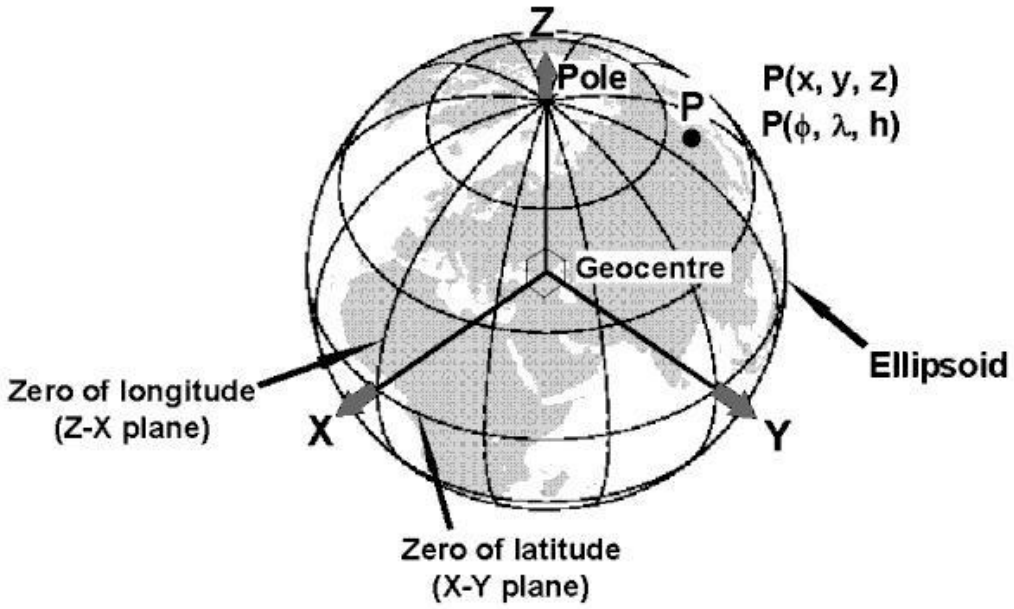

Figure 25: Earth-Centered Earth-Fixed (ECEF) Coordinate system.

Note that, its axes are aligned with the international reference pole (IRP) and international reference meridian (IRM) that are fixed with respect to the surface of the Earth.

The Z-axis extends through True North, which does not coincide with the instantaneous Earth rotational axis. The slight "wobbling" of the rotational axis is known as polar motion. The X-axis intersects the sphere of the Earth at 0° latitude (the equator) and 0° longitude (prime meridian in Greenwich). This means that ECEF rotates with the Earth, and therefore coordinates of a point fixed on the Earth surface do not change.

ECEF coordinates are expressed in a reference system that is related to mapping representations. Due to the complex shape of the Earth, an accurate method for approximating it should be used. Reference ellipsoids permit the conversion from the ECEF coordinates to a more commonly used geodetic-mapping coordinates of Latitude, Longitude and Altitude (LLA). Geodetic coordinates can then be converted to a second map reference known as Mercator Projections, where smaller regions are projected onto a flat mapping surface (that is Universal Transverse Mercator UTM or the USGS Grid System).

4.2. EARTH-CENTERED INERTIAL (ECI):

Earth-Centered Inertial (ECI) coordinate frames have their origins at the centre of mass of the Earth. ECI frames are called inertial because they do not move along with the rotation of the Earth, in contrast to the Earth-Centered, Earth-Fixed (ECEF) frames which rotate in inertial space in order to remain fixed with respect to the surface of the Earth. It is convenient to represent the position and velocities of terrestrial objects in ECEF coordinates or with Latitude, Longitude and Altitude (LLA) because they are placed over the Earth, and using ECI for represent it will be confusing. However, for objects in space, the equations of motion that describe orbital motion are simpler in a non-rotating frame such as ECI. The ECI frame is also useful for specifying the direction towards celestial objects.

The centre of mass of the Earth is accelerating as it travels in its orbit around the Sun, producing that the ECI coordinate frames will not be exactly inertial. In many cases, it may be assumed that the ECI frame is inertial without adverse effect. However, the acceleration of the ECI frame must be considered when computing the gravitational influence of a third body such as the Moon on the dynamics of a spacecraft.

It is convenient to define the orientation of an ECI frame using the Earth's orbit plane and the orientation of the Earth's rotational axis in space. The Earth's orbit plane is called the

ecliptic, and it does not coincide with the Earth's equatorial plane. The angle between the Earth's equatorial plane and the ecliptic, ε, is called the obliquity of the ecliptic and $\varepsilon \approx 23.4^{\circ}$.

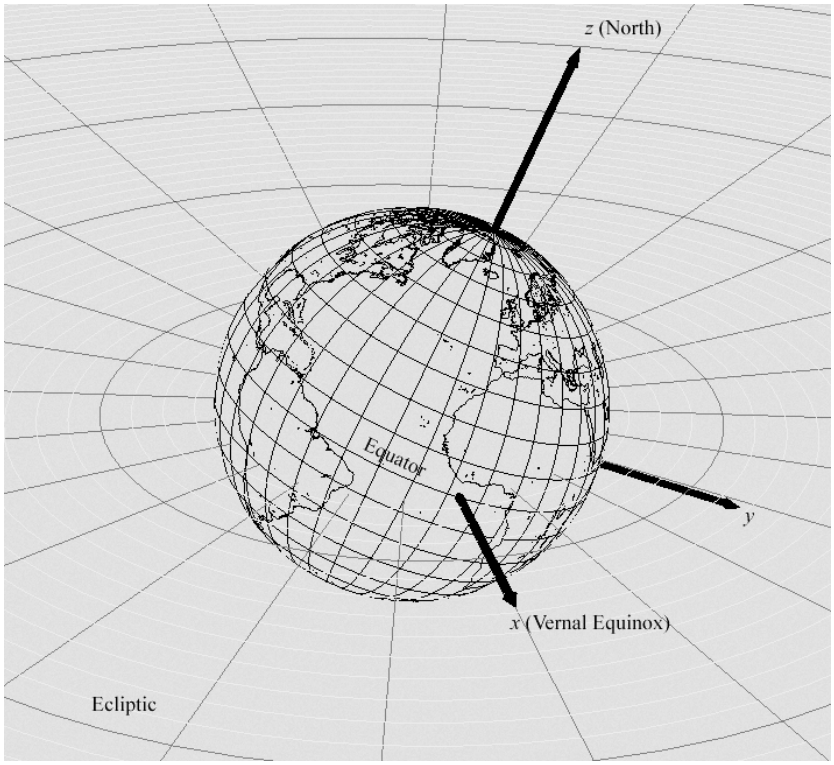

Figure 26: Earth-Centered Inertial (ECI) coordinates system.

An equinox occurs when the Earth is at a position in its orbit such that a vector from the Earth towards the Sun points to where the ecliptic intersects the celestial equator. The equinox which occurs near the first day of spring is called the vernal equinox. The vernal equinox can be used as a principal direction for ECI frames. The Sun lies in the direction of the vernal equinox around the 21st of March. The fundamental plane for ECI frames is usually either the equatorial plane or the ecliptic.

The location of an object in space can be defined in terms of right ascension and declination which are measured from the vernal equinox and the celestial equator. Right ascension and declination are spherical coordinates analogous to longitude and latitude,

respectively. Locations of objects in space can also be represented using Cartesian coordinates in an ECI frame.

The vernal equinox, the equatorial plane of the Earth, and the ecliptic plane vary according to date and are specified for a particular epoch. An epoch is a moment in time used as a reference point for some time-varying astronomical quantity, such as the celestial coordinates or elliptical orbital elements of a celestial body, because these are subject to perturbations and vary with time.

4.3. UNIVERSAL TRANSVERSE MERCATOR (UTM) COORDINATE SYSTEM:

The Universal Transverse Mercator (UTM) conformal projection uses a 2-dimensional Cartesian coordinate system for giving locations on the Earth's surface. Like the traditional method of Latitude and Longitude, it is a horizontal position representation, i.e. it is used to identify locations on the Earth independently of vertical positions. However, it differs from that method in several respects.

The UTM system is not a single map projection. The system instead divides the Earth into sixty zones, each being a six-degree band of longitude, and uses a secant transverse Mercator projection in each zone.

The UTM system divides the Earth between 80°S and 84°N latitude into 60 zones, each 6° of longitude in width. Zone 1 covers longitude 180° to 174° W; zone numbering increases eastward to zone 60, which covers longitude 174°E to 180°.

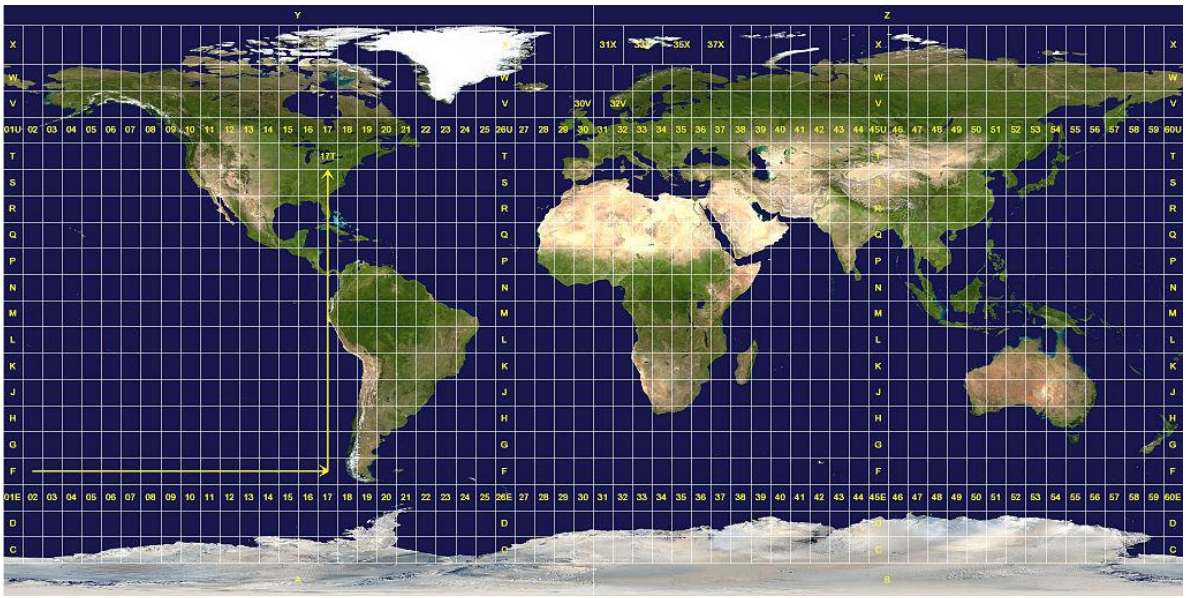

Figure 27: Universal Transverse Mercator (UTM) grid.

Each of the 60 zones uses a transverse Mercator projection that can map a region of large north-south extent with low distortion. By using narrow zones of 6° of longitude (up to 800 km) in width, and reducing the scale factor along the central meridian the amount of distortion is held below 1 part in 1000 inside each zone. Distortion of scale increases at the zone boundaries along the equator.

Each zone is segmented into 20 latitude bands. Each latitude band is 8 degrees high and is lettered starting from “C” at 80°S, increasing up the English alphabet until “X”, omitting the letters “I” and “O” (because of their similarity to the numerals one and zero). The last latitude band, “X”, is extended an extra 4 degrees, so it ends at 84°N latitude, thus covering the northernmost land on Earth.

Latitude bands “A” and “B” do exist, as do bands “Y” and “Z”. They cover the western and eastern sides of the Antarctic and Arctic regions respectively. A convenient mnemonic to remember is that the letter “N” is the first letter in “northern hemisphere”, so any letter coming before “N” in the alphabet is in the southern hemisphere, and any letter “N” or after is in the northern hemisphere.

A grid zone is defined by the combination of a zone and a latitude band. The zone is always written first, followed by the latitude band. For example, a position in Barcelona, Spain, would find itself in zone 31 and latitude band “T”, thus the full grid zone reference is “31T”.

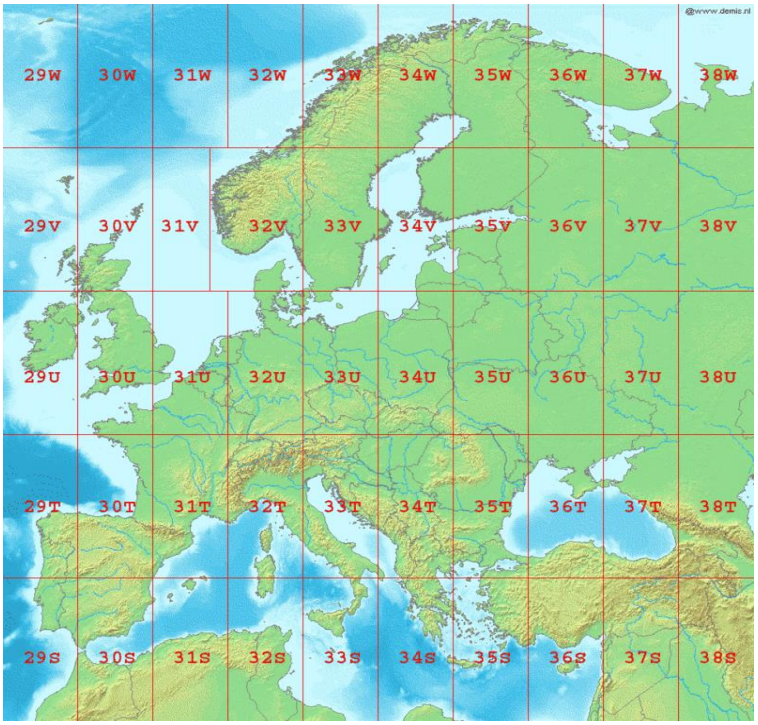

Figure 28: Europe UTM Grid zones.

5. BACK PROJECTION ALGORITHM:

All the concepts applied in this section are extracted from references [6] to [14].

5.1. SYSTEM DEFINITION:

In order to analyse the Back Projection Algorithm in a realistic case, we will consider a bistatic system with the receiver on ground and the satellite on a geosynchronous orbit. In that case, we should take into account that there are different ranges which are important in order to obtain the focused image:

- $R_{Tx-SCENE}$ → Distance between the satellite which is also the transmitter and any point on the scene.
- $R_{Rx-SCENE}$ → Distance between the receiver which is placed on ground and any point on the scene.
- R_{Tx-RX} → Distance between the transmitter (satellite) and the receiver (on ground).

In the next figure we can see the geometry of the system:

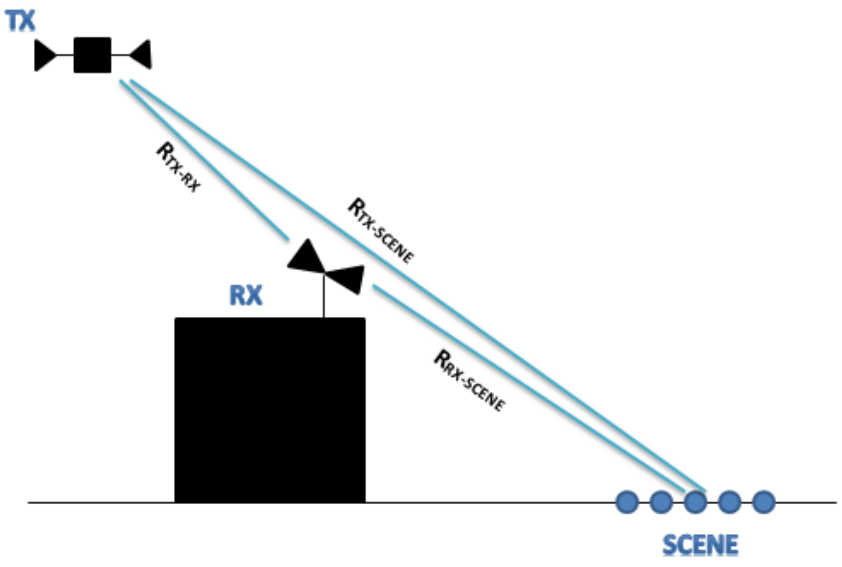

Figure 29: Geometry of a bistatic system with receiver on ground.

5.2. BACK PROJECTION ALGORITHM DEFINITION:

Back Projection Algorithm is the simplest image formation algorithm. In the next figure the block diagram of the Back Projection algorithm it is shown:

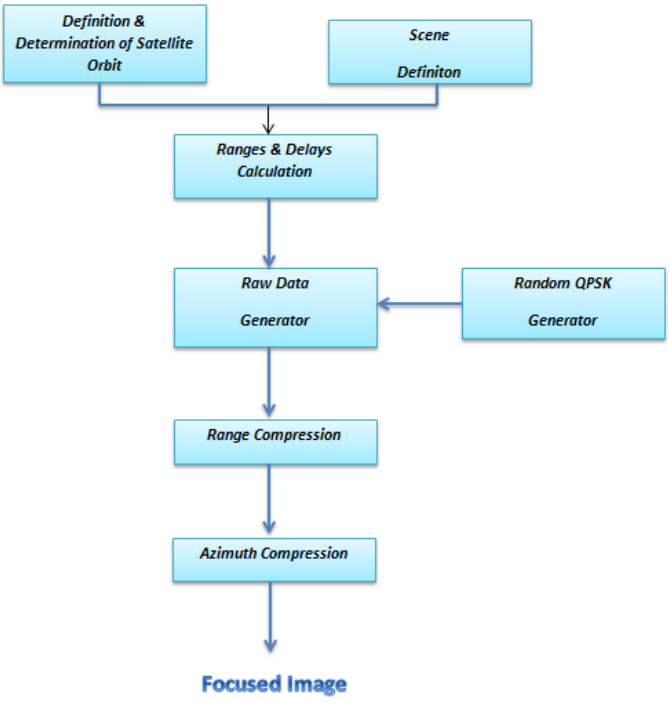

Figure 30: Back Projection Algorithm Schematic.

A brief description of every block is presented next:

- Definition & Determination of Satellite Orbit: obtaining the positions of the satellite in the geostationary orbit.
- Scene Definition: defining the positions of all the points of the scene.
- Ranges & Delays Calculation: calculating the range and the delay between the satellite and each point of the scene for each satellite position.
- Random QPSK Generator: simulating the signal obtained from a TV satellite which results to be a Quadrature Phase Shift Keying.
- Raw Data Generator: generating the matrix which contains the weighted and delayed signals for each satellite position and point on the scene.
- Range Compression: compressing the energy of the signal in the range direction.
- Azimuth Compression: compressing the energy of the signal in the azimuth direction.

5.3. BACK PROJECTION VS FREQUENCY DOMAIN METHODS:

Frequency-domain methods make varying assumptions about squint, range curve migration, platform motion, point spread homogeneity and others. Time-domain back projection, on the other hand, makes few assumptions. The main assumption it makes is that the imaging geometry is known precisely. Because back projection makes fewer assumptions and can model the ideal SAR matched filter, with respect to the frequency-domain methods it enjoys a number of advantages which are extracted from the reference [20] and listed below:

1. Invariant to imaging mode: back projection utilizes the same algorithm regardless of imaging mode. Frequency domain methods, on the other hand, typically require modification depending on the imaging mode and geometry. For example, a different algorithm is used for strip map and spotlight modes. Many of the frequency domain methods require special processing steps when the illumination footprint has non-zero Doppler centroid or for highly squinted geometries.
2. Indifference to unambiguous aliasing in azimuth: ambiguous azimuth aliasing occurs, when along-track frequencies exceed the Nyquist spatial sampling requirements. Unambiguous aliasing occurs in squinted geometries where the signal bandwidth does not exceed the sampling requirements but has undergone "spectral wrapping". Given the pulse repetition frequency (PRF) is high enough to avoid ambiguous signal aliasing in Doppler (i.e., azimuth), back projection is insensitive to the number of spectral wraps that occur in squinted geometries.
3. Space/time matched filter: Back projection fully uses information about the imaging geometry to produce pixel-by-pixel varying matched filter to approximate the expected return signal. This includes higher order effects such as antenna gain compensation (phase and magnitude) on an individual pulse basis. The frequency domain methods can only roughly compensate for higher order effects as they are convolution based and thus use the same response across the entire processing window.

4. Motion compensation: implicit in the back projection algorithm is motion compensation that utilizes available ground information. This advantage becomes more significant at lower airborne altitudes (is not the case we are studying).
5. Multi-static imaging: Multi-static imaging geometries where transmit and receive antennas are widely separated with incongruous motion (e.g., two platforms moving in non-parallel paths) are incompatible with most traditional methods. Back projection handles these situations gracefully (given the positions are known).
6. Ground-plane imaging: orthorectification is a process that maps slant-plane SAR imagery to the ground-plane. It is often necessary post-image formation step to correct image perspective for human visualization. Back projection explicitly images in the ground-plane making the orthorectification step unnecessary. Topography can be explicitly included, which reduces image artefacts due to terrain relief. Frequency domain methods implicitly image the target scene in the slant-plane and therefore require orthorectification.
7. Swath width: Back projection places no fundamental limits on imaging swath other than those imposed by the geometry and physics of the radar (e.g., minimum PRF, etc.). Back projection is able to handle geometries where the relative velocity between the antenna and the scene varies across the imaging swath. Frequency domain methods are commonly limited in these regards.
8. Pulses may be processed as they are received without buffering: Frequency Domain methods involve, as the name implies, performing a transform to the frequency domain and accordingly must buffer a certain amount of data. This may constitute a considerable amount of memory depending on the synthetic aperture length. Back projection can process each pulse as it is received without the need for any additional buffering of the raw data.
9. Azimuth segmentation: when convolving two signals where one is very long, the "overlap and save" method, also called azimuth segmentation, is often used which segments the longer signal and performs the convolution in steps, saving a portion

of the result and discarding the rest. Not only does backprojection not require azimuth segmentation because the output image may be one continuous array, but this may also lead to better continuity between images when placed adjacently. As the frequency domain methods are convolution based they require azimuth segmentation.

10. Image subset: Back projection easily handles imaging a subset of a scene with great computational improvement (equivalent to the percentage of pixels not imaged). Frequency domain methods generally require all the pixels contributing to the scene to be imaged simultaneously, or have limited computational savings when imaging a subset of the scene.
11. Simplicity: of all the SAR image formation algorithms, back projection may have the simplest description of them all. With range-compressed data as the input, back projection may be described with one equation denoted by the summation of two terms. Only the range-Doppler algorithm without motion compensation, range curvature migration compensation, or secondary range compression approaches this level of simplicity.

While the backpropagation algorithm exhibits a remarkable number of advantages over the frequency domain methods, it has an important disadvantage: computational expense. Computational complexity has traditionally been the limiting factor preventing the wide adoption of back projection for SAR image formation. In recent years however, advancement in computational capabilities has rendered this disadvantage, all but obsolete as current technology allows back projection images in real time. This leaves as the principle disadvantage to use back projection the requirement of knowing precisely the image geometry.

Back projection requires the time-varying position of the antenna(s) be known relative to the three-dimensional position of the imaged terrain in the ground-plane of the scene. The position of the antenna is usually estimated with an Inertial Navigation System (INS) while the height of the scatterers is satisfied through the use of a digital elevation map (DEM). In contrast, while frequency domain methods require knowledge of the antenna

position for motion compensation and imaging (i.e., an INS is necessary), only the slant-plane projection of the position of the scatterers is needed, which is implicit in the radar data. Frequency domain processing thus can be done adequately without a DEM.

5.4. DESCRIPTION OF THE ALGORITHM:

In this section the different blocks that compound the algorithm will be described in detail:

- Scene Definition.
- Determination of the Satellite Orbit.
- Ranges and Delay calculation.
- Random QPSK generation.
- Raw Data generator.
- Range Compression.
- Azimuth Compression.

Note that the Determination of the Satellite Orbit block is already performed and it is extracted from the PFC of Marc Fernandez Uson "Orbit Determination Methods and Techniques". In this algorithm we are using his code in order to generate a geostationary Keplerian orbit.

5.4.1. SCENE DEFINITION:

In the next figure we are able to observe the scene that is taken as an example in order to prove that the back projection algorithm is valid for obtaining focused images from a opportunity geosynchronous satellite.

The steps that are taken in order to define the scene are the next ones:

1. First of all we define the position of the receiver antenna. In our case this antenna is placed in the roof of the D3 building. (Note we should find its UTM coordinates).
2. Next, we need to define the width and length of the scene. In our case the length and the width are equal and equal to 200 m.
3. Next, we should define the step between two pixels of the image. In our case this step should be 5 meters, as the expected range resolution is 5 meters.

4. Once we have this information we should find the UTM coordinates of the top-left corner of the scene. We should propagate these coordinates in order to obtain the UTM coordinates of each point of the scene.
5. Now we have the UTM coordinates of the entire scene. Then, we can pass these UTM coordinates into LLA coordinates (Latitude, Longitude and Altitude).
6. Finally, we pass the LLA coordinates of each point of the scene into ECEF coordinates (Earth Centered, Earth Fixed).

Figure 31: Scene Definition.

RX Antenna Coordinates	
UTM E(x)	425728 m
UTM N(x)	4582314 m
Latitude	41° 23’ 20.195”
Longitude	2° 6’ 41.832”

Table 5.1. RX antenna Coordinates (UTM and LLA).

5.4.1.1. UTM TO LLA:

Note that for converting UTM coordinates on some known ellipsoid, we should use the next equations. Note that these equations are an approximation.

$$\phi = \phi_1 - \left(R_{N_1}\frac{\tan\phi_1}{R_1}\right)\left[\frac{D^2}{2} - (5 + 3T_1 + 10C_1 - 4C_1^2 - 9e'^2)\frac{D^4}{24} + (61 + 90T_1 + 298C_1 + 45T_1^2 - 252e'^2 - 3C_1^2)\frac{D^5}{720}\right] \quad (5.1)$$

$$\lambda = \lambda_0 + \frac{D - (1 - 2T_1 + C_1)\frac{D^3}{6} + (5 - 2C_1 + 28T_1 - 3C_1^2 + 8e'^2 + 24T_1^2)\frac{D^5}{120}}{\cos\phi_1} \quad (5.2)$$

Where C_1, T_1, R_{N_1} and R_1 are C, T, R_N and R_m calculated at the footprint latitude ϕ_1.

$$\phi_1 = \mu + \left(3\frac{e_1}{2} - 27\frac{{e_1}^2}{32} + \cdots\right)\sin(2\mu) + \left(21\frac{{e_1}^2}{16} - 55\frac{{e_1}^4}{32} + \cdots\right)\sin(4\mu) + \left(151\frac{{e_1}^3}{96} + \cdots\right)\sin(6\mu) + \left(1097\frac{{e_1}^4}{512}\right)\sin(8\mu) + \cdots \quad (5.3)$$

Where:

$$\mu = \frac{M_0 + \frac{y}{k_0}}{a\left(1 - \frac{e^2}{2} - 3\frac{e^4}{64} - 5\frac{e^6}{256} - \cdots\right)} \quad (5.4)$$

$$e_1 = \frac{1 - \sqrt{1 - e^2}}{1 + \sqrt{1 - e^2}} \quad (5.5)$$

5.4.1.2. LLA TO ECEF:

The conversion between the two reference coordinate systems can be performed using closed formulas (although iteration methods also exist). The closed formulas are showed below:

$$X = (N + H)\cos\phi\cos\lambda \qquad (5.6)$$

$$Y = (N + H)\cos\phi\sin\lambda \qquad (5.7)$$

$$Z = \left(\frac{b_2}{a_2}N + h\right)\sin\phi \qquad (5.8)$$

Where:

- h -> ellipsoidal height (Geodetic).
- H -> orthometric height (MSL).
- N -> Geoid separation (undulation).

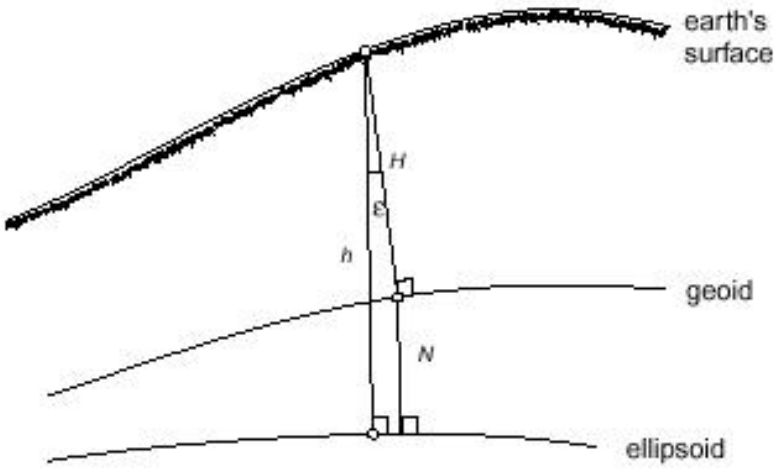

Figure 32: Ellipsoid and MSL Reference Datum's.

5.4.3. RANGES AND DELAY CALCULATION:

Once we have the scene defined and the orbit calculated, we need the ranges between each position of the satellite and each point of the scene. In order to do that we should apply the Euclidean distance formula:

$$d(p,q) = d(q,p) = \sqrt{(q_1 - p_1)^2 + (q_2 - p_2)^2 + \cdots + (q_n - p_n)^2}$$

$$= \sqrt{\sum_{i=1}^{n} (q_i - p_i)^2} \qquad (5.9)$$

Note that the Euclidean distance or Euclidean metric is the "ordinary" (i.e. straight-line) distance between two points in Euclidean space. With this distance, Euclidean space becomes a metric space. The associated norm is called the Euclidean norm. Older literature refers to the metric as Pythagorean metric. A generalized term for the Euclidean norm is the L^2 norm or L^2 distance.

Alternatively, it follows from (6.9) that if the polar coordinates of the point p are (r_1, θ_1) and those of q are (r_2, θ_2) then the distance between points is:

$$d(p,q) = \sqrt{r_1^2 + r_2^2 - 2r_1 r_2 \cos(\theta_1 - \theta_2)} \qquad (5.10)$$

Now, if the position of the satellite at each epoch is stated as $(x_{sat}, y_{sat}, z_{sat})$ and the position one point of the scene is stated as $(x_{scene}, y_{scene}, z_{scene})$, then the range between them is calculated using the formula (6.9) as:

$$r_{sat-scene} = \sqrt{(x_{sat} - x_{scene})^2 + (y_{sat} - y_{scene})^2 + (z_{sat} - z_{scene})^2} \qquad (5.11)$$

Finally, if the position of the receiver is stated as (x_{rx}, y_{rx}, z_{rx}), the distance between satellite and receiver and between receiver and a point on the scene are:

$$r_{sat-rx} = \sqrt{(x_{sat} - x_{rx})^2 + (y_{sat} - y_{rx})^2 + (z_{sat} - z_{rx})^2} \qquad (5.12)$$

$$r_{rx-scene} = \sqrt{(x_{rx} - x_{scene})^2 + (y_{rx} - y_{scene})^2 + (z_{rx} - z_{scene})^2} \qquad (5.13)$$

Then, once we have got the distances (note that only the distances are needed in order to apply the back projection algorithm), we are able to calculate the delays in time.

First of all, the delay between a point of the scene and the receiver antenna is calculated as:

$$t_{rx-scene} = \frac{r_{rx-scene}}{c} \qquad (5.14)$$

Then, the delay between the satellite and a point of the scene is calculated as:

$$t_{sat-scene} = \frac{r_{sat-scene}}{c} \qquad (5.15)$$

An important delay is the one that represents the path between the satellite and a point of the scene in both directions. That is:

$$t_{2way-sat-scene} = \frac{2 \cdot r_{sat-scene}}{c} \qquad (5.16)$$

Finally, the delay of the path satellite-scene-receiver that is the delay in which we should receive each echo of the signal scattered by the scene:

$$t_{tot} = \frac{r_{sat-scene} + r_{rx-scene}}{c} = t_{sat-scene} + t_{rx-scene} \qquad (5.17)$$

Note that $(x_{sat}, y_{sat}, z_{sat})$, $(x_{scene}, y_{scene}, z_{scene})$ and (x_{rx}, y_{rx}, z_{rx}) should be expressed in the same coordinate system. That is, if the state vector of the satellite is expressed in ECI (Earth Centered Inertial), the others should be also expressed in ECI. On the other hand, if the state vector of the scene is expressed in ECEF (Earth Centered, Earth Fixed), the others should be also expressed in ECEF.

5.4.3.1. ECI TO ECEF:

ECI has fixed axes with respect to the "celestial sphere", and thus its axes do not rotate with the rotation of the Earth (or it's back and forth wobbling, but let's approximate the "wobble" as zero for simplicity). ECEF fixes the x (and therefore, by orthogonality, y) axis with respect to the Earth rotation.

Therefore, this is a change from a non-rotating reference frame (ECI) to a rotating reference frame (ECEF). This is nothing more than a change of basis. Recall from Linear Algebra that the formula for a change of basis is simply $C \cdot x = B \cdot y$, where C is the matrix composed of the basis vectors of reference frame 2, x is the vector in reference frame 2, B is the matrix composed of the basis vectors of reference frame 1 and y is the initial vector.

Going from ECI to ECEF is easy because we can establish B with the Cartesian basis vectors i, j and k, meaning that B is the identity matrix. That simplifies $C \cdot x = B \cdot y$, into $C \cdot x = y$, so all we need to do to find x is define C, and then find it's inverse.

Because ECI and ECEF are both 3-D coordinate systems, B and C are 3x3 matrices, and x and y are 3x1 matrices (column vectors).

We would like a C that is an orthogonal matrix (i.e. the columns are orthonormal to each other, so the norm of each is 1, and the inner product of the columns is zero). It has to represent a system that is rotating on its z –axis at a constant rotational velocity, say ω.

If you were looking at the Earth from Polaris (the North Star), you would see counter-clockwise rotation. So the ECEF x-axis starts pointing in ECI's +x direction, rotates towards ECI's +y , then towards ECI's –x, then towards ECI's –y, and back to ECI's +x. if you break this down into components, ECEF's x-axis starts pointing at (1,0) in ECI, then goes to (0,1), then (-1,0), etc., so the first coordinate here goes $1 \to 0 \to -1$ (like the cosine function) and the second coordinate goes $0 \to 1 \to 0 \to -1$ (like the sine function).

That means the first column vector in C is $\vec{c}_1$:

$$\vec{c}_1 = \begin{bmatrix} \cos \omega t \\ \sin \omega t \\ 0 \end{bmatrix} \qquad (5.18)$$

Using the same process for the y-axis, we can get the second column vector in C:

$$\vec{c}_2 = \begin{bmatrix} -\sin \omega t \\ \cos \omega t \\ 0 \end{bmatrix} \qquad (5.19)$$

The third column vector is easy, as the z-axis doesn't really change between the two reference frames, so it's just:

$$\vec{c}_3 = \begin{bmatrix} 0 \\ 0 \\ 1 \end{bmatrix} \qquad (5.20)$$

So finally the C matrix results:

$$C = \begin{bmatrix} \cos \omega t & -\sin \omega t & 0 \\ \sin \omega t & \cos \omega t & 0 \\ 0 & 0 & 1 \end{bmatrix} \qquad (5.21)$$

With that matrix we are able to change an ECI vector into an ECEF vector, which is important in order to express the state vectors of the satellite, the scene and the receiver in the same reference frame.

5.4.4. RANDOM QPSK GENERATOR:

As we will use an opportunity satellite as the transmitter of our satellite system, we should simulate a random QPSK generator because the TV broadcast satellites use this modulation in order to transmit signals. Note that this is not the typical case, because the communication satellites use to transmit pulsed signals, like a chirp. Then, our back projection simulator will use a LFSR to generate a stream of bits in order to select them in pairs for forming the symbols of the QPSK constellation.

5.4.4.1. QUADRATURE PHASE-SHIFT KEYING (QPSK):

Phase-shift keying (PSK) is a digital modulation scheme that conveys data by modulating the phase of a reference signal (the carrier wave). Varying the sine and cosine inputs at a precise time, we generate the modulation. It is widely used for wireless LAN's, RFID and Bluetooth communication.

Any digital modulation scheme uses a finite number of distinct signals to represent digital data. In the case of a PSK it uses a finite number of phases; each assigned a unique pattern of binary digits. Usually, each phase encodes an equal number of bits. Each pattern of bits forms the symbol that is represented by the particular phase.

Quadrature Phase-shift Keying (QPSK) uses four points on the constellation diagram, equispaced around a circle. With four phases, QPSK can encode two bits per symbol. In the next figure we are able to see the position of the points used to minimize the bit error rate (BER).

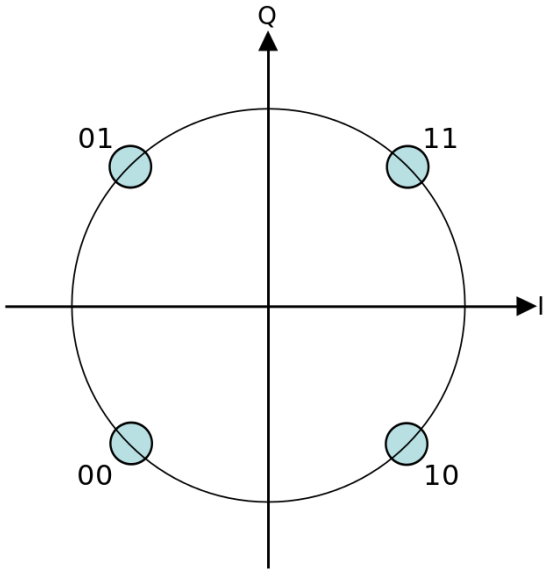

Figure 33: Constellation diagram for QPSK with Gray coding. Each adjacent symbol only differs by one bit.

The mathematical analysis shows that QPSK can be used either to:

- Double the data rate compared with a BPSK system while maintaining the same bandwidth.
- Maintain the data-rate of BPSK but halving the bandwidth needed. In this latter case, the BER of QPSK is exactly the same as the BER of BPSK.

Given that radio communication channels are allocated giving a prescribed (maximum) bandwidth, the advantage of QPSK over BPSK becomes evident: QPSK transmit twice the data rate in a given bandwidth compared to BPSK – at the same BER. The engineering penalty that is paid is that QPSK transmitters and receivers become more complicated than the ones for BPSK. However, with modern electronics technology, the penalty cost is very moderate.

5.4.4.2. LINEAR FEEDBACK SHIFT REGISTERS (LFSR):

A Linear Feedback Shift Register (LFSR) is a shift register whose input bit is a linear function of previous states. The initial value of the LFSR is usually called the seed. If we choose the feedback function, we will be able to produce a bit sequence that seems random due to it extremely long cycle, despite the fact that it is not completely random.

Linear Feedback Shift Registers can be implemented in two ways. The Fibonacci implementation consists of a simple shift register in which a modulo-2 sum of the binary weighted taps is fed back to the input. The modulo-2 sum of two 1-bit binary numbers results 0 if the two numbers are identical, and 1 if they are different.

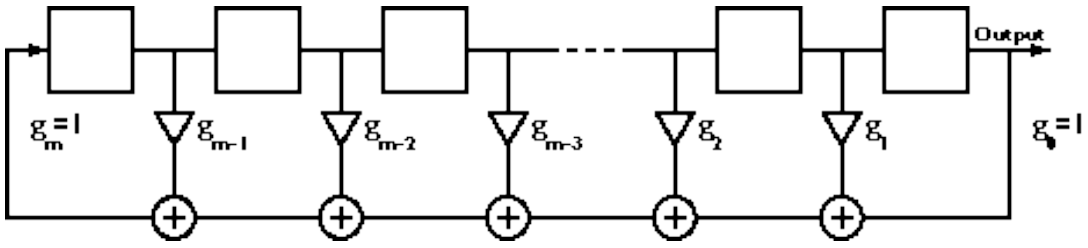

Figure 34: Fibonacci implementation of LFSR. Source: New Wave Instruments "LFSR".

For any given tap, weight g_i is either 0, meaning "no connection" if it is not fed back or 1, if it is fed back. Two exceptions are g_0 and g_m, which are always 1 and thus always connected. Note that g_m is not really a feedback connection, it is the input of the LFSR system.

The Galois implementation consists of some shift register, the which contents are modified at every step by the binary-weighted values of the output stage, again using modulo-2- math.

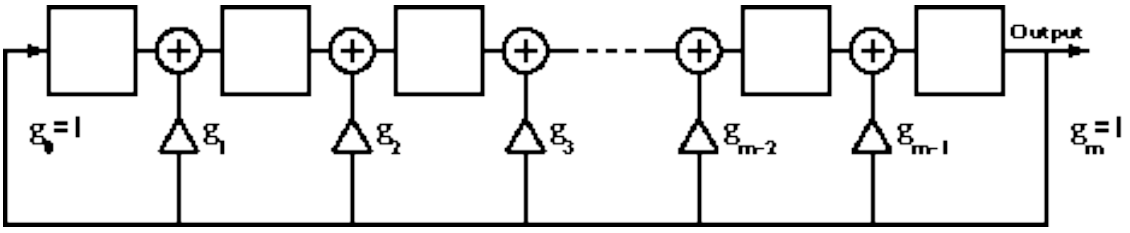

Figure 35: Galois implementation of LFSR. Source: New Wave Instruments "LFSR".

The same sequence will be produced by both systems if they are fed back with identical weights. However, the initial states of the two implementations must necessarily be different for the two sequences in order to have identical phase. The initial state of the Fibonacci form is normally called the initial fill or initial vector, and it comprises the first m bits output from the generator. The initial state of the Galois generator should be properly adjusted to obtain the equivalent output of its first m bits. In mathematical literature, the initial state of either form is called the seed as previously said.

In order to implement modulo-2 sum, XOR (Exclusive-OR) gates should be used. The Galois form is generally faster than the Fibonacci in hardware due to the reduced number of logic gates in the feedback loop, thus making it the preferred LFSR implementation.

A given set of feedback connections can be expressed in a convenient and easy-to-use shorthand form, with the connection numbers being listed inside a pair of square brackets. In doing so, connection g_0 is not listed, since is always connected. Although g_m is always connected, it is listed in order to easily express the shift register size (i.e. the number of registers).

A set of feedback connections, or taps, is denoted as $[f_1, f_2, f_3, \ldots, f_J]$ where the subindex J is the total number of feedback taps (not including g_0), f_1 = m is the highest-order feedback tap (and the size of the LFSR), and f_j represent the remaining feedback taps. The value of each f_j is equal to the subindex of the corresponding connection g.

A set of feedback taps specified in this format is called a feedback tap set, feedback set or feedback pattern. As an example, the [7, 5 3, 2] feedback set would signify a seven-step shift register with feedback connections at taps g_7, g_5, g_3, g_2 and as always at g_0.

A related convention is that an LFSR with m shift register states is said to be an Rm LFSR. For example, an R6 generator is one with six stages.

5.4.4.3. MAXIMAL LENGTH SEQUENCES:

LFSR generators generate what are called Linear Recursive Sequences (LRS) because all operations are linear. The number of feedback taps and the initial state determine the length of the sequence before repetition. An LFSR of any given size m (number of registers) is capable of producing every possible state during the period $N = 2^m - 1$ shifts, but will do so only if the proper feedback taps have been chosen. For example, such an six stage LFSR will contain every possible combination of ones and zeros after 63 shifts. Such a sequence is called a maximal length sequence, maximal sequence, or less commonly, maximum length sequence. It is often abbreviated as m-sequence. M-sequences are often referred to as pseudo noise (PN) or pseudorandom sequences, because they present optimal noise-like characteristics.

Technically speaking, maximal length sequences can actually produce two sequences:

1. The first (the trivial one) has a length of one, and occurs when the initial state of the generator is set to all zeros. The generator simply remains in the zero state indefinitely.
2. The other one (the useful one) has a length of $2^m - 1$.

Together, these two sequences account for all 2^m states of an m-bit state register.

If the feedback taps used on an LFSR are non-maximal, it will not produce an m-sequence, and the length of the sequence generated will depend on the initial state.

Properties of non-maximal sequences are generally worse to those of maximal sequences. So avoiding non-maximal sequences is a common practice.

Any LFSR can be represented as a polynomial of variable X, referred to as the generator polynomial:

$$G(X) = g_m X^m + g_{m-1} X^{m-1} + g_{m-2} X^{m-2} + \cdots + g_2 X^2 + g_1 X + g_0 \qquad (5.22)$$

The coefficients g_i represent the tap weights, as defined in Figures 38 and 39, and are 1 for taps that are connected (fed back), and 0 otherwise. The order of the polynomial m, represents the number of LFSR stages. Rules of linear algebra apply to the polynomial, but all mathematical operations are performed in modulo-2.

To sum up, a list of the m-sequences properties is presented:

1. An m-bit register produces an m-sequence of period $2^m - 1$.
2. An m-sequence contains exactly $2^{(m-1)}$ ones and $2^{(m-1)} - 1$ zeros.
3. The modulo-2 sum of an m-sequence and another phase (i.e. time-delayed version) of the same sequence yields yet a third phase of the sequence. Note that, each stage of an m-sequence generator runs through some phase of the sequence. While this is obvious with a Fibonacci LFSR, it may not be with a Galois LFSR.
4. A sliding window of length m, passed along an m-sequence for $2^m - 1$ positions, will span every possible m-bit number, except all zeros, once and only once. That is, every state of an m-bit state register will be encountered, with the exception of all zeros.
5. Define a run of length r to be a sequence of r consecutive identical numbers, bracketed by non-equal numbers. Then in any m sequence there are:
    a. 1 run of ones of length m.

b. 1 run of zeros of length m-1.

c. 1 run of ones and 1 run of zeros, each of length m2.

d. 2 runs of ones and 2 run of zeros, each of length m-3.

e. 4 runs of ones and 4 runs of zeros, each of length m-4.

f. …

g. 2^{m-3} runs of ones and 2^{m-3} runs of zeros, each of length 1.

6. If an m-sequence is mapped to an analogue time-varying waveform, by mapping each binary zero to -1 and each binary one to +1, then the autocorrelation function for the resulting waveform will be unity for zero delay, and $-1/(2^m - 1)$ for any delay greater than one bit, either positive or negative in time. The shape of the autocorrelation function between -1 bit and +1 bit will be triangular, centred on time 0. That is, the function will rise linearly from time equal minus one bit to time 0, and then decline linearly from time 0 to time equals plus one bit.

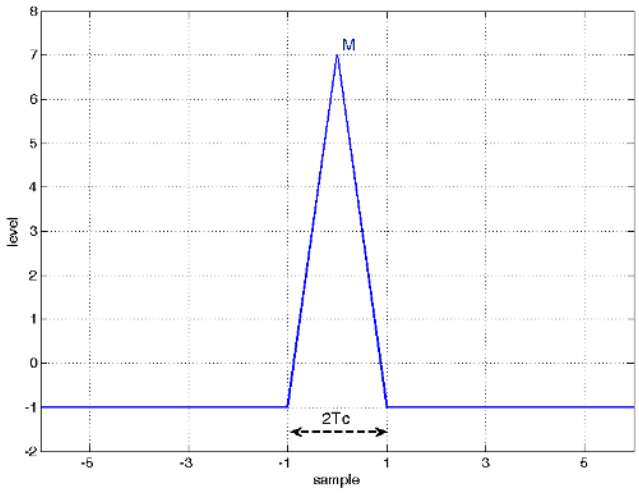

Figure 36: M-sequence autocorrelation.

Other interesting facts regarding m-sequences and feedback sets that produce them include the following:

a. A time reversal of the original sequence can be generated reversing the order of the feedback taps. Note that this time-reversed sequence is also an m-sequence.
b. It is not possible to generate a m-sequence using an odd number of taps (including g_m, but never g_0).

5.4.4.4. BIT STREAM QPSK GENERATION:

The purpose of this algorithm block is to generate a bitstream which will be used for generating the symbols of the QPSK signal used for generating the raw data.

A bitstream is a sequence of bits. In order to generate that bitstream we will use a LFSR which generates an m-sequence of the desired length. Note that the m-sequence will be treated as the bitstream.

Once we have the bitstream, the only thing we should do is take the bits in pairs, and classify them depending on which bits they are:

- If the pair of bits is '00' we will have the QPSK symbol '1'.
- If the pair of bits is '01' we will have the QPSK symbol 'j'.
- If the pair of bits is '10' we will have the QPSK symbol '-1'.
- If the pair of bits is '11' we will have the QPSK symbol '-j'.

Doing that we are transforming a pseudorandom bitstream just formed by ones and zeros, into a pseudorandom QPSK signal which emulates the signal we will receive from an opportunity satellite illuminating our target scene.

5.4.5. RAW DATA GENERATOR:

Raw Data (sometimes called source data or atomic data) is data that has not been processed for a use. A distinction is sometimes made between data and information to the effect that information is the end product of data processing (in our case, the focused image obtained by the back projection algorithm). Raw data that has undergone processing is sometimes referred to as cooked data.

Although raw data has the potential to become "information", it requires selective extraction, organization and sometimes analysis and formatting for presentation.

First of all we should define a parameter that will be used later in the raw data generator block. This parameter is called wavelength number or wavenumber, and it is the spatial frequency of a wave, either in cycles per unit distance or radians per unit distance. It can be envisaged as the number of waves that exist over a specified distance (analogous to frequency being the number of cycles or radians per unit time).

$$k_0 = \frac{2\pi}{\lambda} = \frac{2\pi}{c/f} \qquad (5.23)$$

Note that in our case, our raw data should be the signal that is received in the receiver antenna which is compound of the different echoes that scatters the scene. Our raw data should be a matrix in which every row is a different satellite position and every column is a different arrival delay. So we will have for each row a different signal formed by the different echoes of the scene.

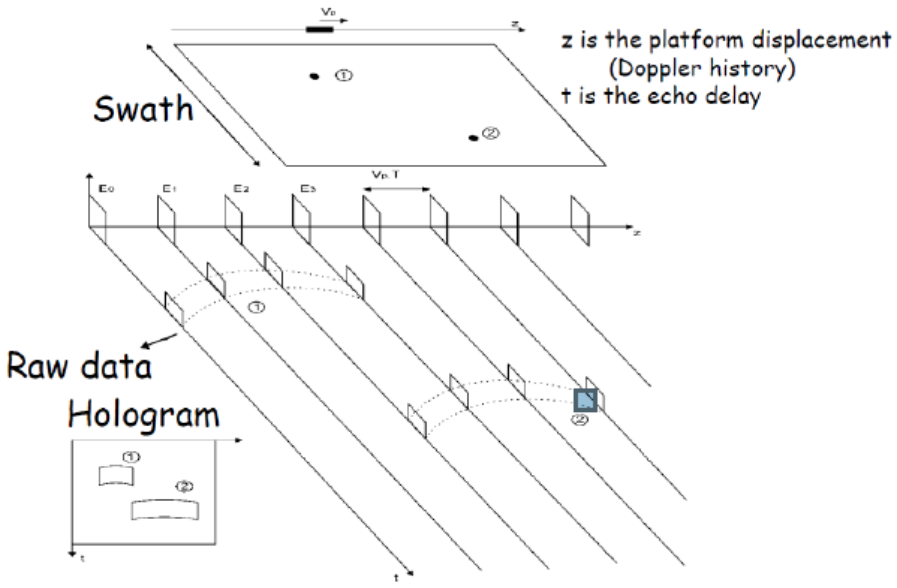

Figure 37: The raw data acquired by a SAR. In t axis the samples of the echoes of a transmitted Chirp pulse along range and in z axis the azimuth samples. Source: Antoni Broquetas Ibars.

In the previous figure we can see an example of raw data, but in this case the transmitted signal is not a continuous bitstream, it is a Chirp pulse. In our case the acquisition of raw data becomes a little bit more complicated due to the fact that we have data before the first received echo. Due to the fact that we are simulating this problem we cannot generate an infinite QPSK symbol stream. Our stream is limited and firstly we will not have data (QPSK symbols) before the first received echo, but we will need to generate this data.

In order to generate this non-existing data, we will need to find the number of symbols necessary for filling the empty part of the raw data matrix.

$$\#\ past\ samples = \left\lceil \frac{\Delta t}{T_s} \right\rceil = \left\lceil \frac{t_{max} - t_{ref}}{T_s} \right\rceil \qquad (5.24)$$

Where t_{max} is the maximum delay taking into account all satellite possible positions that an echo will possibly have, t_{ref} is the delay between the satellite and the receiver antenna and T_s is the time of symbol of the QPSK stream.

Once we have generated this "past data" we will concatenate it with the already existing QPSK symbol stream like it is showed in the next figure:

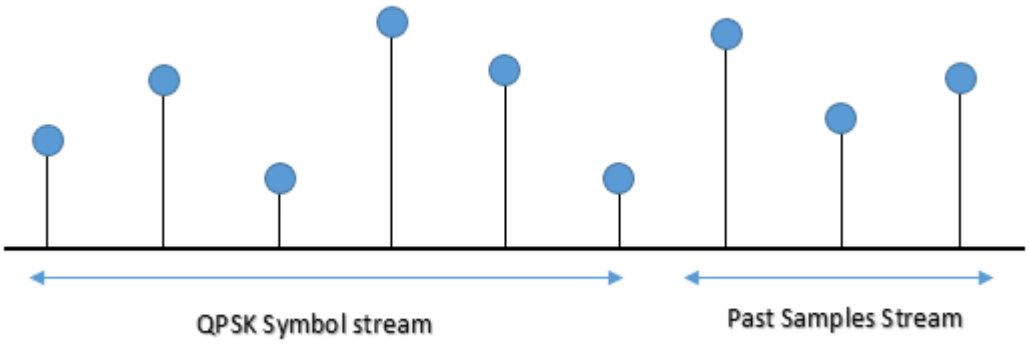

Figure 38: QPSK Symbol stream and Past Samples stream order.

Note that the past samples stream is concatenated just behind the QPSK symbol stream this is done in that way due to a property of the interpolation method that will be used in order to do the displacement for simulating the delayed echoes. This property will be seen in the next paragraphs.

Finally, we are ready for generating the raw data. In order to do that we should apply the next formula, which takes into account the scattering coefficients of the scene and the delays that the echoes will have:

$$RD_i = \sum_i \hat{s}(t - t_i) = \varphi_i \cdot s(t - t_i) \cdot e^{-jk_0(R_{sat-scene} + R_{RX-scene})} \qquad (5.25)$$

Where i is the subscriber of each point of the scene, φ_i is the scattering coefficient of each point of the scene, t_i is the total delay of the path between the satellite, each point of the scene and the receiver antenna, k_0 is the wavenumber of the signal transmitted, $R_{sat-scene}$ is the range between the satellite and each point on the scene and $R_{RX-scene}$ is the range between each point of the scene and the receiver antenna.

Note that performing a delay is not a trivial operation in MatLab when it is not a multiple of the sampling period. We should apply a method of interpolation using the properties of the FFT, and that is the reason why we concatenate the past samples behind the QPSK symbol stream, due to the fact that when we make the displacements of the signal samples, this later samples will pass to the beginning of the stream (circular behavior).

$$s(t) \xrightarrow{FFT} S(f) \cdot e^{-j2\pi\omega\, t_r} \xrightarrow{FFT^{-1}} s(t - t_r) \qquad (5.26)$$

$$s[n] \xrightarrow{FFT} S[k] \cdot e^{j2\pi\frac{1}{NT_s}kt_r} \xrightarrow{FFT^{-1}} s[k - m] \qquad (5.27)$$

Applying the formula on (5.27) we are able to delay the QPSK symbol stream m samples, performing a delay in the signal.

$$m = \frac{t_r}{NT_s} \qquad (5.28)$$

Where t_r is the total delay of the path between the satellite, the desired point of the scene and the receiver antenna, N is the total number of symbols in the QPSK symbol stream and T_s is the time of symbol.

But take care because this operation changes depending if the number of symbols of the QPSK symbol stream is even or odd.

If it is even we will have:

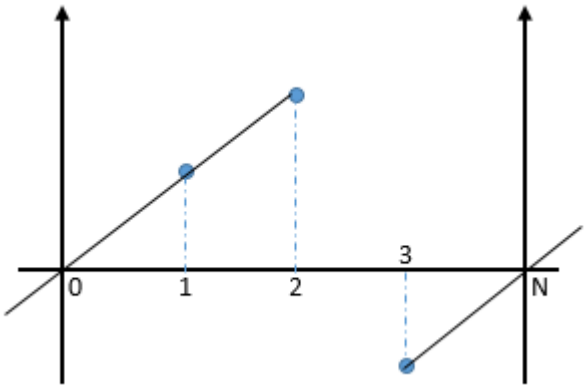

Figure 39: FFT displacement for even number of symbols.

$$e^{-j2\pi\frac{1}{NT_s}kt_r} \quad for\ k \in \left[0, \frac{N}{2}\right] \rightarrow \quad Positive\ Part \qquad (5.29)$$

$$e^{-j2\pi\frac{1}{NT_s}(k-N)\,t_r} \quad for\ k \in \left[\frac{N}{2}+1, N\right] \rightarrow \quad Negative\ Part \qquad (5.30)$$

On the other hand, if it is odd we will have:

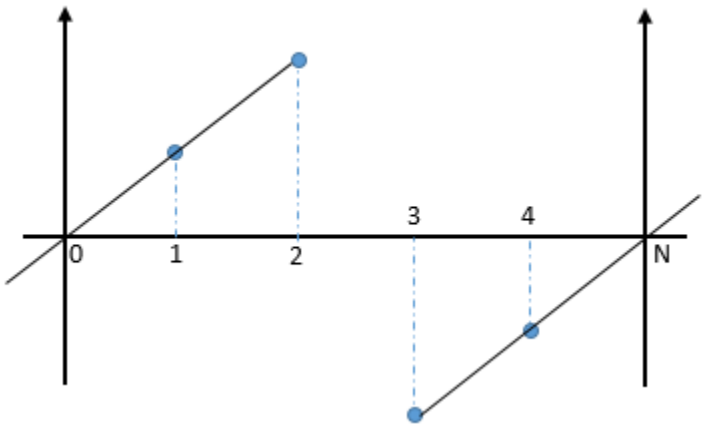

Figure 40: FFT displacement for odd number of symbols.

$$e^{-j2\pi\frac{1}{NT_s}k\,t_r} \quad for\ k \in \left[0, fix\left(\frac{N}{2}\right)-1\right] \rightarrow \quad Positive\ Part \qquad (5.31)$$

$$e^{-j2\pi\frac{1}{NT_s}(k-N)t_r} \quad for\ k \in \left[fix\left(\frac{N}{2}\right)+1, N\right] \rightarrow \quad Negative\ Part \qquad (5.32)$$

Applying that formulas depending on the parity of the QPSK symbol stream we can displace its samples in order to generate a delay, and in that way obtain the raw data signal for each position of the satellite.

In the next figure we can see an example on how the raw data will look like without the addition of those past samples needed:

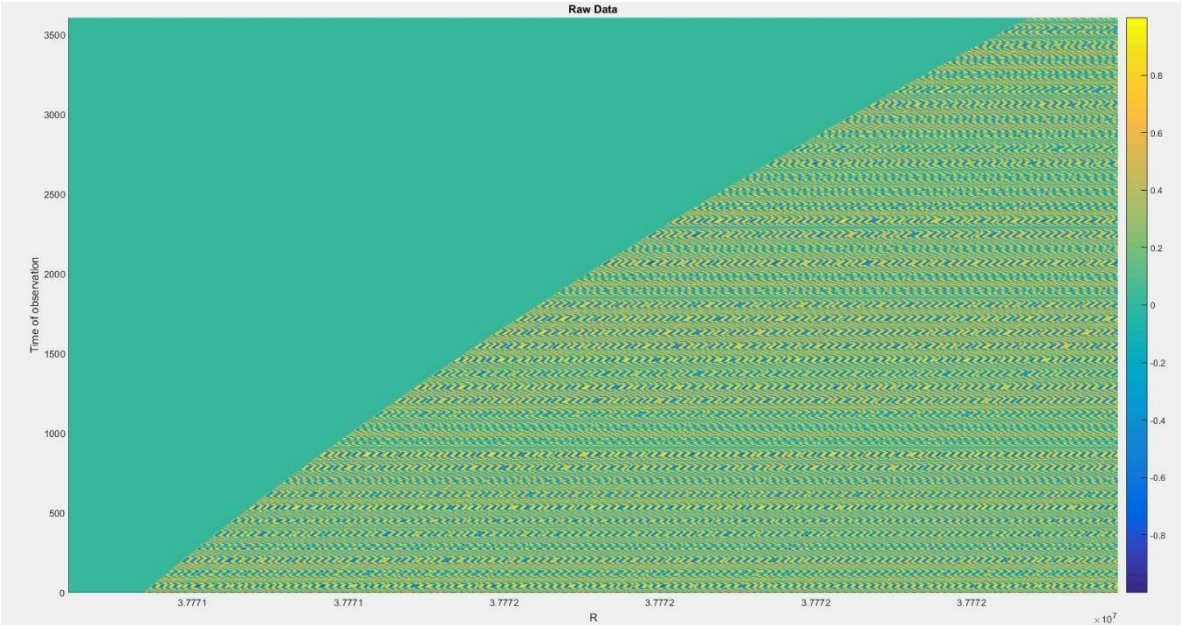

Figure 41: Raw Data Amplitude without the addition of the past samples needed. Acquisition done during 1 hour taking 1000 possible satellite positions.

Note that saving all the information that the raw data generation block will generate it is not trivial because the amount of information that it will produce will vary significantly depending on the azimuthal resolution you want/need to achieve. In order to avoid that problem, the algorithm use a solution that is take only the raw data matrix of the proper satellite position and then apply the range and azimuth compression in order to obtain a pre-image. Once the algorithm has done this for one satellite position it can jump to the next one and so on. Finally the only thing the algorithm has to do is properly add all the pre-images obtained and correctly weighted.

In the next section we will see more results and we will analyze them.

5.4.6. RANGE COMPRESSION:

Once we have the raw data is time to process it in order to obtain the focused image which is the desired result of our back projection algorithm. First of all we should apply a range compression method to it.

The range compression technique is based on the matched filter.

5.4.6.1. MATCHED FILTER:

The matched filter is a filter whose impulse response, or transfer function is determined by a certain signal, in a way that will result in the maximum attainable signal to noise ratio [14]. In order to compress the raw data into a relative narrow pulse a matched filter will be used in the range compression step.

A matched filter is designed to maximize the response of a linear system to a particular known signal. The next figure (Figure 43) shows the basic block diagram of a matched filter radar system. The transmitted waveform is generated by a signal generator designated as s(t). The signal output from s(t) is amplified, fed to antenna, radiated, reflected from a target and return to receiver. The output of receiver is fed into a matched filter after suitable amplification. The matched filter impulse response, h(t), is simply a scaled, time reversed and delayed form of the input signal. The shape of the impulse response is related to the signal and therefore matched to the input. The matched filter has the property of being able to detect the signal even in the presence of noise. It yields a higher output peak signal to mean noise power ratio for the input than for any other signal shape with the same energy content.

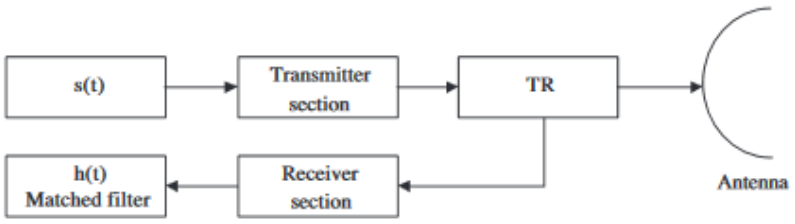

Figure 42: Basic matched filter radar system. Source: [14].

Assuming return signal is a replica of transmitted signal with a time delay t_0. The filter is matched to s(t) and has an impulse response of:

$$h(t) = Ks(t_0 - t) \qquad (5.33)$$

where t_0 is a delay and K is a constant. The Fourier Transform (FT) of the impulse response of h(t) is known as the transfer function of the matched filter, H(jω) and can be written as:

$$H(j\omega) = FT\{h(t)\} = \int_{-\infty}^{\infty} h(t)e^{-j\omega t}dt \qquad (5.34)$$

Substituting h(t) from equation (5.33), we obtain:

$$H(j\omega) = K\int_{-\infty}^{\infty} s(t_0 - t)\, e^{-j\omega t}dt \qquad (5.35)$$

By changing the time variable as, $\tau = t_0 - t$, (5.35) is given as:

$$H(j\omega) = -K\int_{-\infty}^{\infty} s(\tau)\, e^{j\omega\tau}d\tau \qquad (5.36)$$

The Fourier Transform of s(t) is written as:

$$S(j\omega) = \int_{-\infty}^{\infty} s(\tau)\, e^{-j\omega t}dt \qquad (5.37)$$

The complex conjugate of $S(j\omega)$, $S^*(j\omega)$ is given as:

$$S^*(j\omega) = S(-j\omega) \qquad (5.38)$$

From the equations above, $H(j\omega)$can be expressed as:

$$H(j\omega) = -Ke^{-j\omega t_0}S^*(j\omega) \qquad (5.39)$$

The transfer function of the matched filter obtained is the complex conjugate of the spectrum of the signal to which is matched. Hence, the impulse response h(t) of the matched filter is a scaled, time reversed and delayed version of the desired signal.

The output of a matched filter when a signal, s(t) is impressed at the input can be computed with the expressions derived for the transfer function. In the time domain, the output can be obtained either by the convolution integral or the cross correlation integral. For the convolution integral, let y(t) be the output of the matched filter. The output, y(t), is then given by:

$$y(t) = h(t) * s(t)$$
$$= \int_{-\infty}^{\infty} h(t-u)s(u)du = \int_{-\infty}^{\infty} s(u)s^*(u-t)\,du = R_{ss}(t) \qquad (5.40)$$

This is true only in the case that h(t) is a matched filter.

5.4.6.2. RANGE COMPRESSION ALGORITHM:

Now that we know what is a matched filter we are ready to perform the range compression of the raw data.

Remember that the raw data is stored in a matrix in which rows there are the echo signals from the scene for each satellite position. So, we should apply a matched filter to each of the rows in order to perform the range compression to each one of these signals.

So, for each satellite position we generate a matched filter adapted to the signal received directly at the receiver antenna. Then, we pass the signal reflected by the scene (raw data) for that filter, and in that way we obtain the range compressed signal for each one of the rows of the raw data matrix.

Note that we should calculate a different matched filter for each satellite position, due to the fact that the TV broadcasting satellite is transmitting a different signal depending on the TV images transmitted, and as we want to adapt the matched filter to the received signal at the receiver, we must change the matched filter at each iteration.

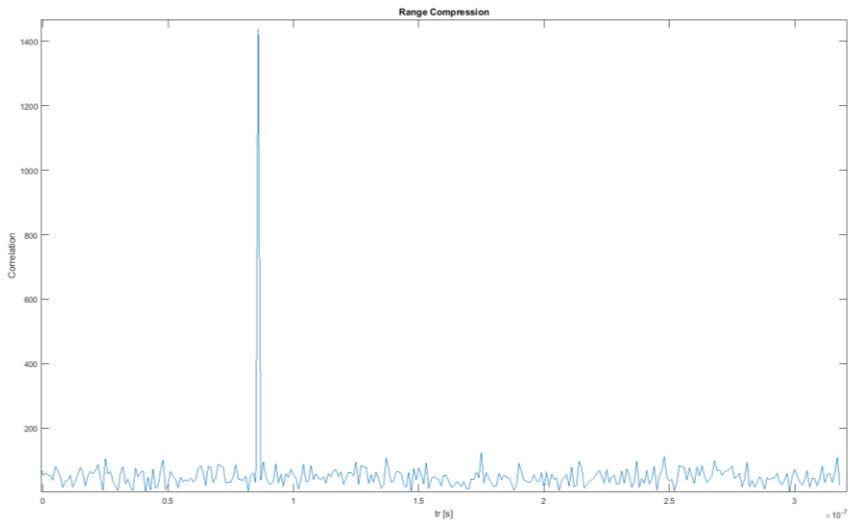

Figure 43: Range Compressed Signal cut. One scatterer placed at the centre of the scene.

On the previous figure (Figure 44) we are able to see a result of a range compressed signal. Note that the energy of the signal is compressed in just one narrow band around the illuminated point of the scene. The x-axis is the delay between the point of the scene and the receiver. The matched filter is doing its purpose because it is compressing the energy of the signal in the desired bands.

In the next section we will see more results and we will analyze them.

5.4.7. AZIMUTH COMPRESSION:

Now, we must transform the range compressed signal of 2 dimensions in an image that fulfils the next condition:

$$\psi_I(r) \approx \psi(r) \qquad (5.41)$$

That is what we will obtain after the back projection algorithm implementation into the azimuth compressor will be performed. The back projection algorithm is based on a coherent addition of the measured data (pixel) by compensating the amplitude and phase lost in the direct problem.

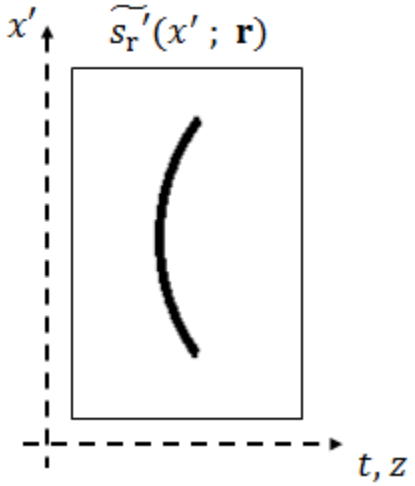

Figure 44: Example of range compressed signal of a single target.

Although the range compressed signal has 2 dimensions, every scene point in the range compressed domain generates a hyperbolic line of data. Thus, we can integrate the compensated amplitude and phase data along this measured compressed data line and derive the final image $\psi_I(r)$ as:

$$\psi_I(r) = \int_{x'} \widetilde{s'}_r[l(x';\boldsymbol{r});\boldsymbol{r}] \frac{4\pi l^2(x';\,\boldsymbol{r})}{\sqrt{\sigma} G[\varphi(x';\boldsymbol{r})]} e^{j2k_0 l(x';\boldsymbol{r})} dx' \qquad (5.42)$$

In the next figure we can see the geometry used to solve the Equation (6.42):

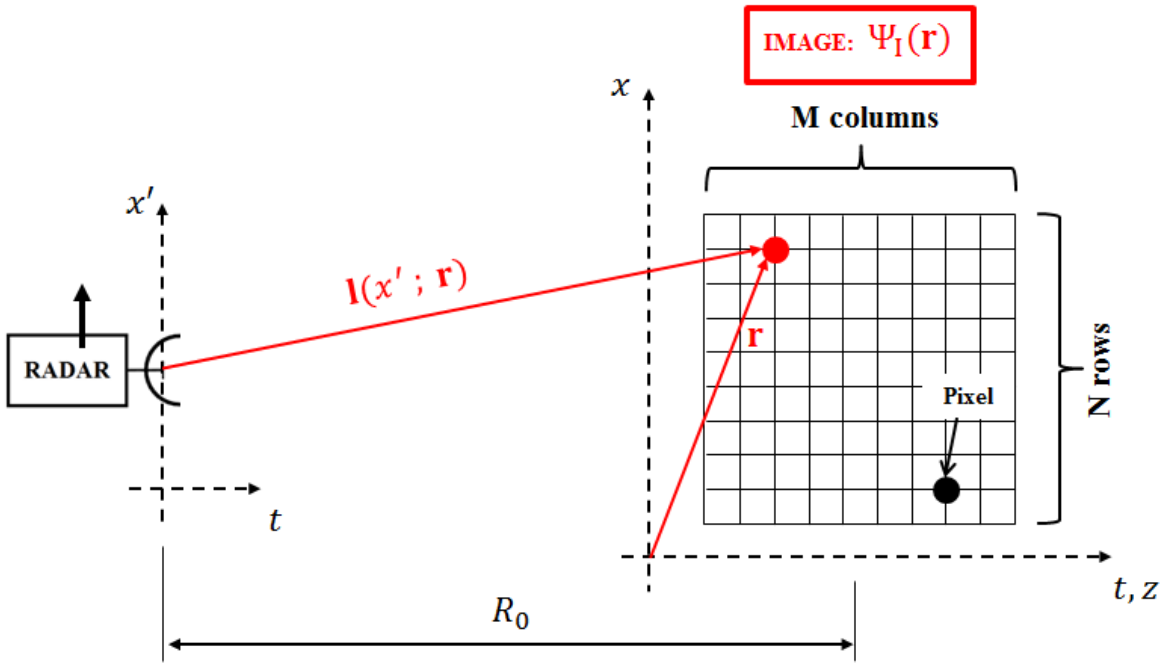

Figure 45: Geometry used in Equation (5.42).

The image will contain NxM pixels. The N and M are values that will depend on the size of the evaluated area $\psi(r)$, and the desired range and azimuth resolutions. The distance l is already computed for each radar antenna position and pixel of the image, and it is used to achieve the appropriate value of the range compressed signal on each case. Therefore, interpolation is needed on this latter step for better accuracy when obtaining the focused image.

Finally that is the last step of the back projection algorithm, using the equation (5.42) we are able to obtain a focused image of the illuminated scene, proving that the back projection algorithm is able to retrieve focused images from geostationary radar.

In the next figure we can see a focused image obtained by this algorithm, using 1000 positions of the satellite during an integration time of 6 hours and with just one desired target on the scene:

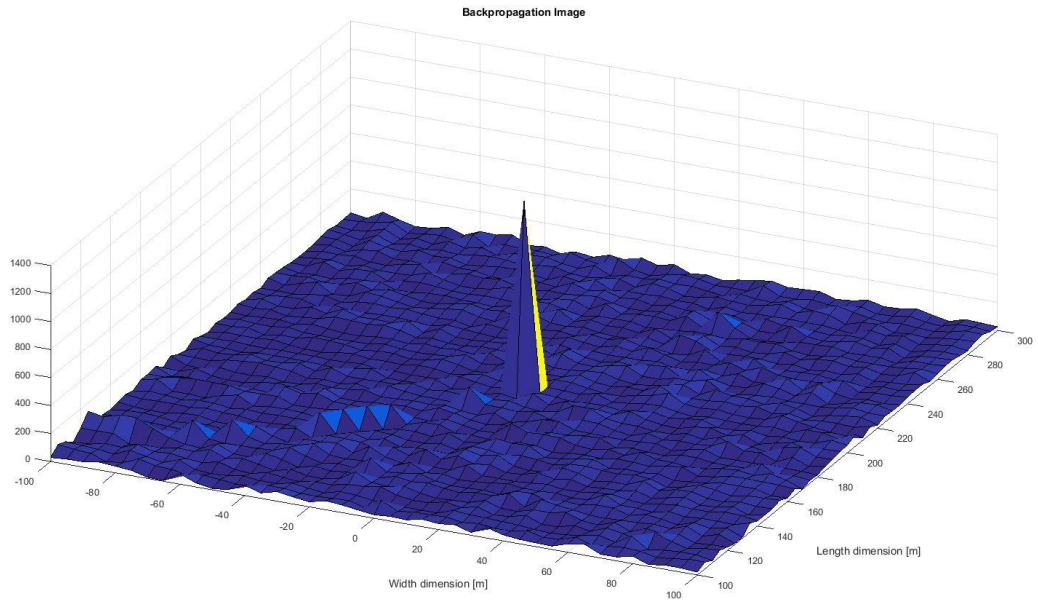

Figure 46: Image obtained with Back Projection Algorithm in 3D.

6. RESULTS:

In this section we will analyse the results obtained by the different blocks of the algorithm.

6.1. QPSK GENERATOR RESULTS:

First of all we will see the autocorrelation of the sequence of bits generated by the LFSR:

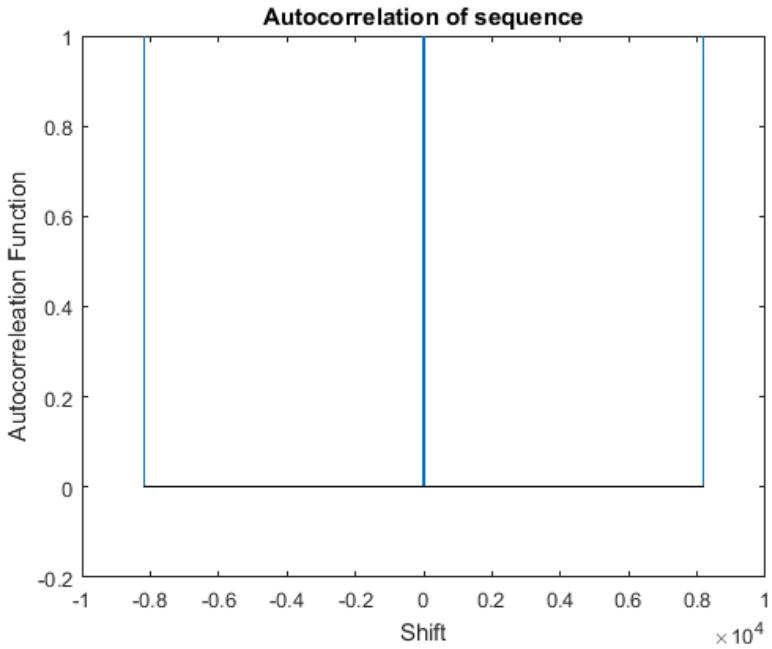

Figure 47: Autocorrelation of the sequence of bits generated by the LFSR Generator.

Now let's see the phase of the sequence of symbols generated by the QPSK generator:

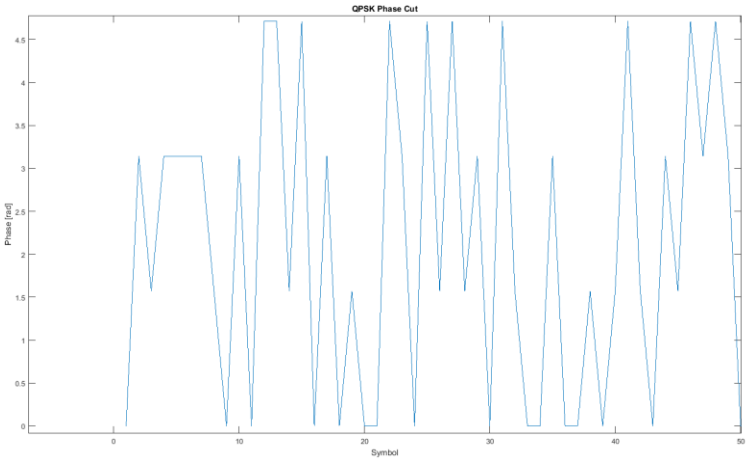

Figure 48: QPSK Phase cut.

As we can see, the only possible phase results for the symbols are the expected ones: 0°, 90°, 180° and 270°. So we are generating the symbols of the QPSK correctly.

In order to prove that the QPSK generator is working properly let's see if the symbols are placed correctly:

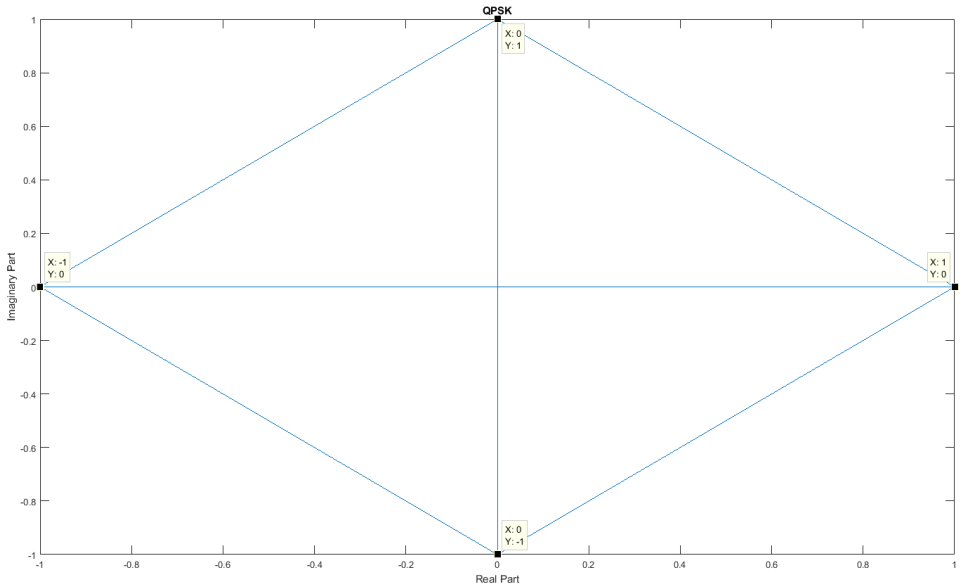

Figure 49: QPSK Constellation

As we can see in the previous figure, the QPSK constellation is correctly done. We are generating the symbols [1], [-1], [j] and [-j]. Note that if we do the absolute value of the QPSK symbol sequence it will be a constant placed to 1. So the phase of the symbols is the difference between them which means the binary information is only in the phase.

6.2. RAW DATA GENERATOR RESULTS:

In the Figure 46 we have a result of a raw data generated but without adding the "past samples" needed in order to simulate that the transmitted signal is a QPSK continuous stream. In this section we will see a result of the phase of the raw data generated by a scene during an integration time of 6 hours using 100 positions of the satellite and with just one target on the scene.

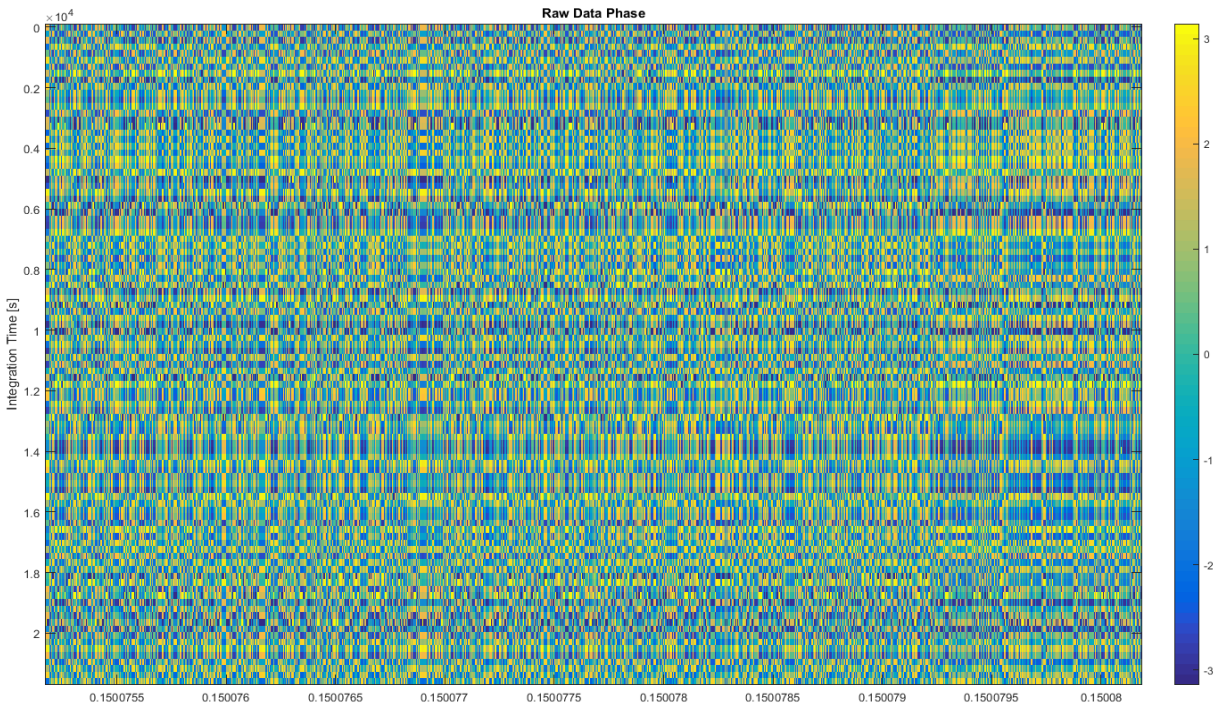

Figure 50: Raw Data Phase generated by a continuous stream of QPSK symbols scattered by a scene with just one target. Integration time of 6 hours and 100 positions of the satellite.

As it is said in a previous section the raw data only does not provide any useful information. That is clear seeing the previous figure.

So we must process this raw data using the range compression and azimuth compression blocks in order to obtain the focused image.

6.3. RANGE COMPRESSION RESULTS:

Let's see the results of the range compression. The range compression compresses the energy of the signal into very narrow bands that in our case should coincide with the position of the targets of the scene.

For example if we place just a target in the middle of the scene, the delay between the reference and the target results to be:

$$t_r = 8.600804127234518e-08\ s$$

So the peak of the range compressed signal for this unique configuration of the scene should coincide with that value. Let's see that in the next figure:

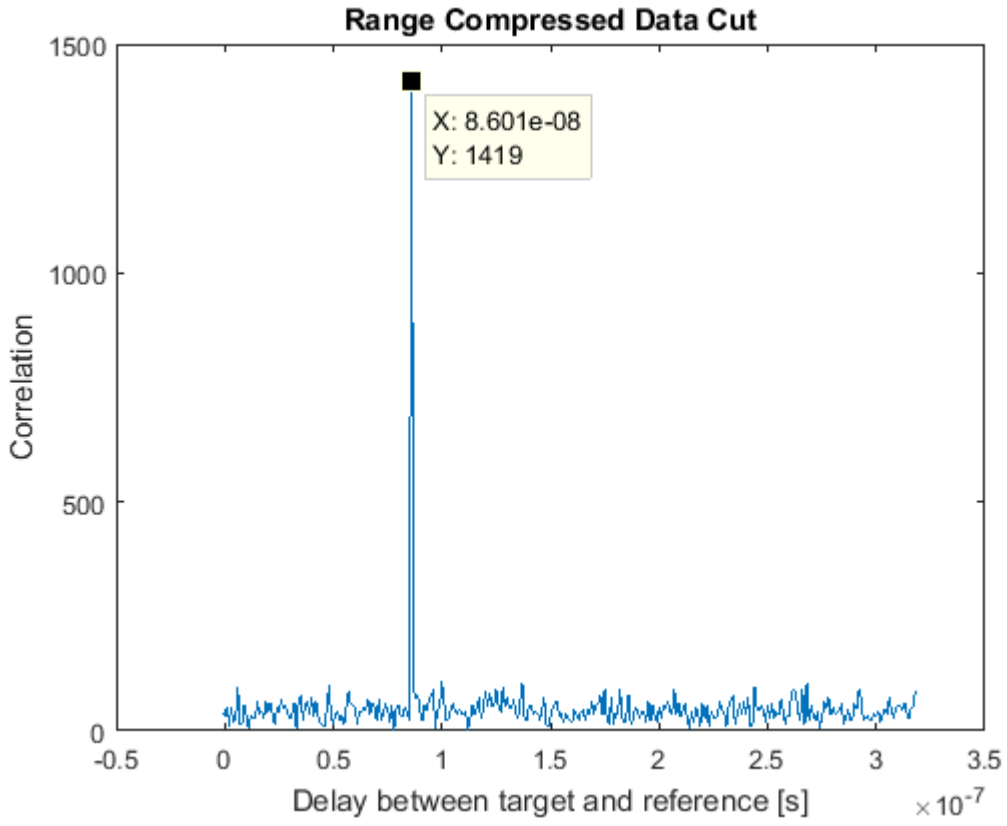

Figure 51: Range Compressed Cut for 1 target on the scene.

As we are able to see the peak of the range compressed signal is exactly the same point where the target is placed.

Let's do the same for a scene with two targets (one placed on the left top corner and another one on the right bottom corner). Its delays are:

$$t_{r_1} = 9.541528839251967e-08\ s$$

$$t_{r_2} = 2.483211022641374e-07\ s$$

Just as before, the peaks of the range compressed signal should coincide with these delays.

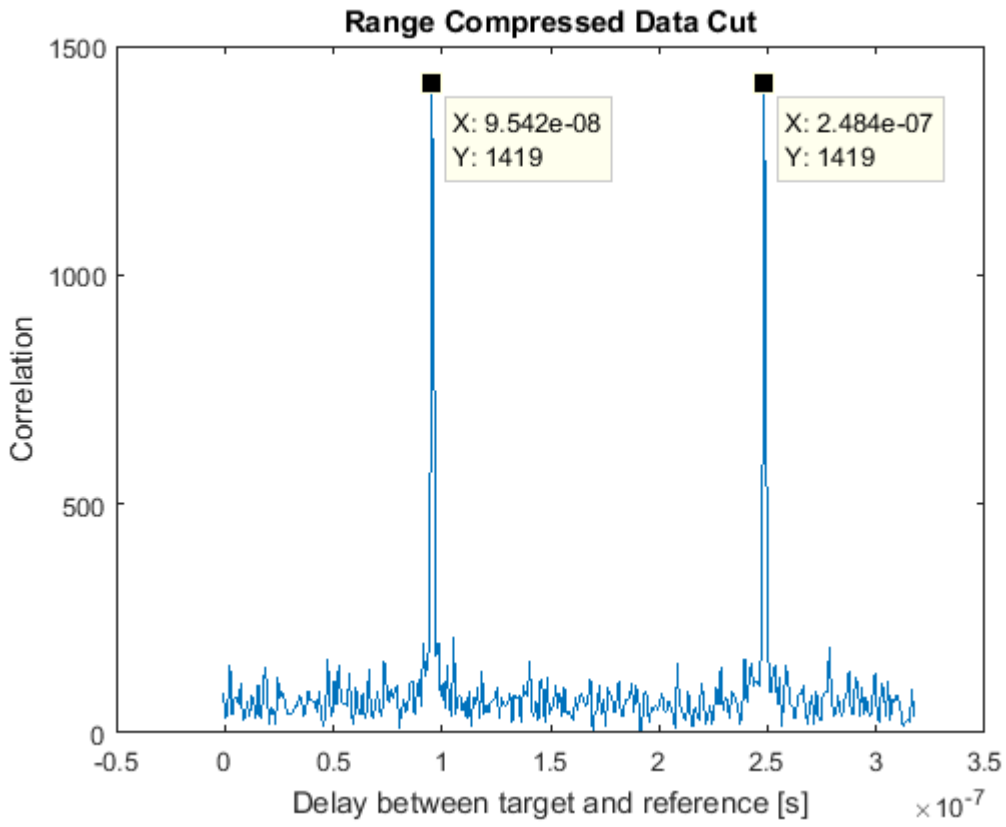

Figure 52: Range Compressed Cut for 2 targets on the scene.

Just as before, the peaks coincide with the position of the targets on the scene.

Finally, we will see what happens if we add more targets to the scene. Let's try the range compression with a scene containing 5 different targets. The delays of the targets are noted next:

$$t_{r_1} = 9.541528839251967e-08\ s$$

$$t_{r_2} = 2.483211022641374e-07\ s$$

$$t_{r_3} = 8.600804127234518e-08\ s$$

$$t_{r_4} = 3.041028689143577e-07\ s$$

$$t_{r_5} = 3.963415159957684e-08\ s$$

Just as before, the peaks of the range compressed signal should coincide with these delays.

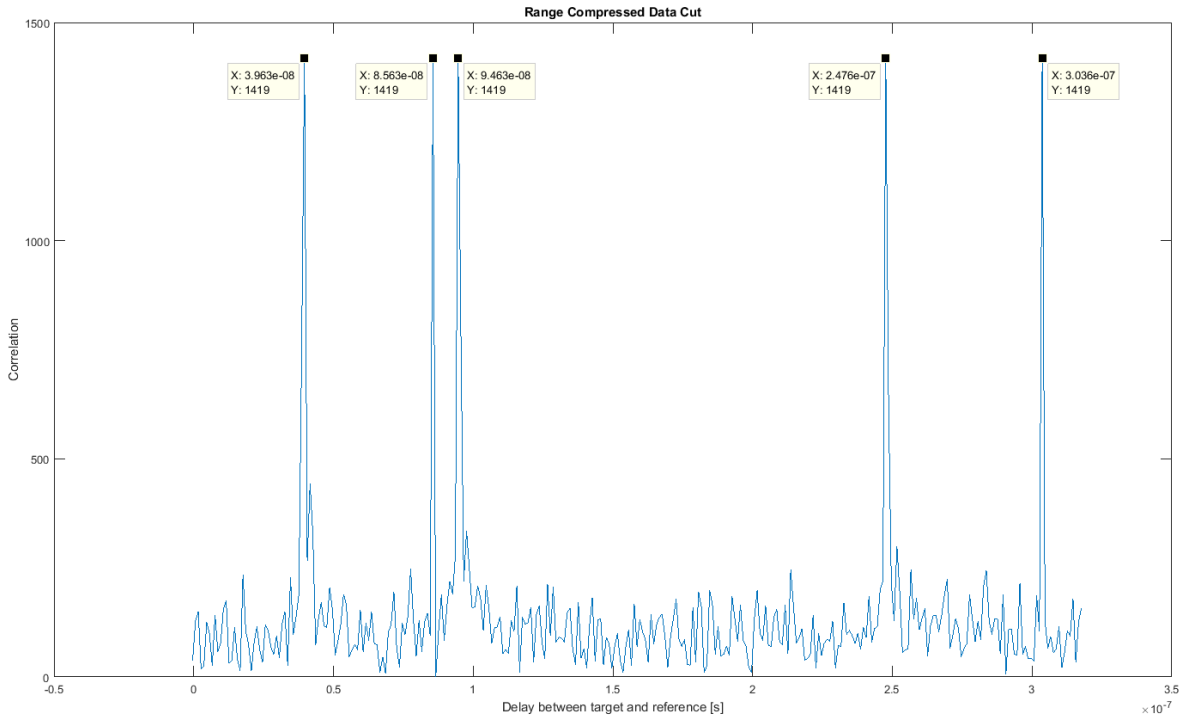

Figure 53: Range Compressed Cut for 2 targets on the scene.

Finally we have proved that despite of the number of targets that the scene contains, the range compressor compresses the energy of the signal in the right bands, that ones near the position of the targets on the scene.

To sum up, the range compressor works properly and how it is expected. In the next sections we will see the final results of the algorithm after performing the azimuth compression that is the focused images.

6.4. AZIMUTH COMPRESSION RESULTS:

In this section we will see the focused images obtained by the back projection algorithm after the azimuth compression.

Let's see the first result for a scene containing just one target on the centre of the scene.

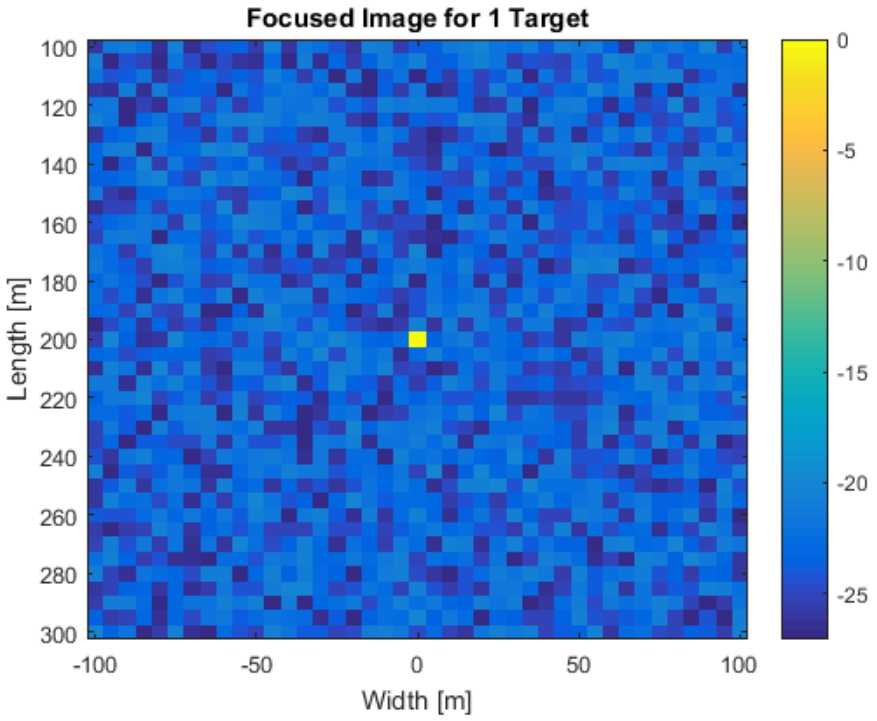

Figure 54: Dynamic Margin of the Focused image of a scene with 1 target.

As we can see the target on the centre of the scene is the highest one while the rest of the scene points are at a noise level approximately 20 dB down the peak level. In the next section we will see which is the minimum target scattering value that we will be able to see with that noise level.

Now let's see a focused image for a scene containing two targets (one on the left bottom corner and the other one on the right top corner):

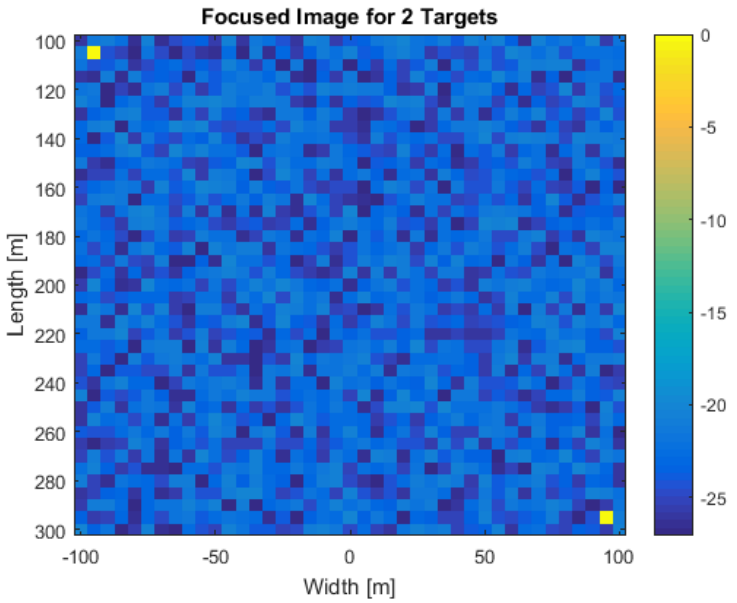

Figure 55: Dynamic Margin of the Focused image of a scene with 2 targets.

Just as before, the noise level is around -20 dB from the value of the peaks. Note that the algorithm is able to focus two different targets on a scene.

Finally and just as in the previous section, we will analyse what happens if we have a scene with some more targets (i.e. 5 targets). The focused image provided by the algorithm for this scene is:

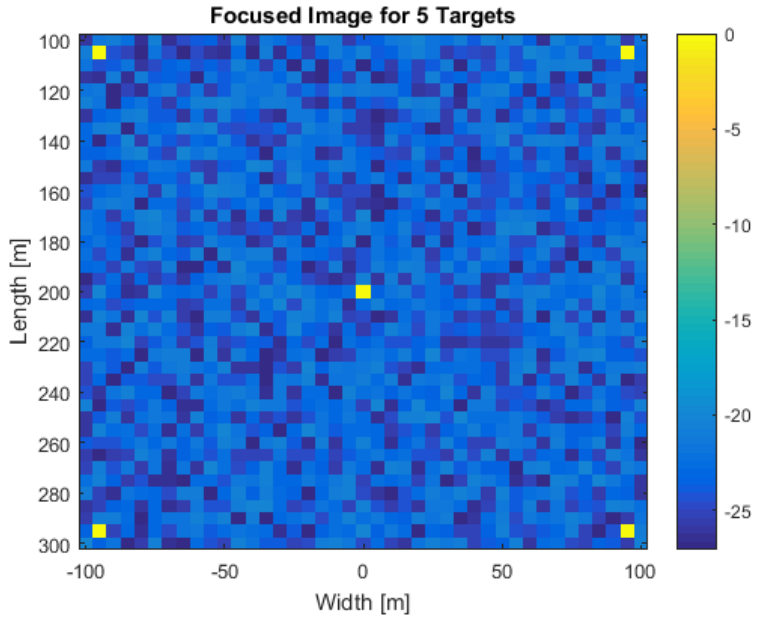

Figure 56: Dynamic Margin of the Focused image of a scene with 5 targets.

6.5. TESTING THE FOCUSED IMAGES:

In the previous section we have seen that the noise level is around -20 dB which is quite low. But let's see which is the minimum scattering value that we will be able to distinguish. For doing that we will place 4 targets on a scene each one with a different scattering value. The scattering values for those targets are listed next:

- Left Top Corner → Scattering value of 1.
- Right Top Corner → Scattering value of 0.5.
- Left Bottom Corner → Scattering value of 0.25.
- Right Bottom Corner → Scattering value of 0.125.

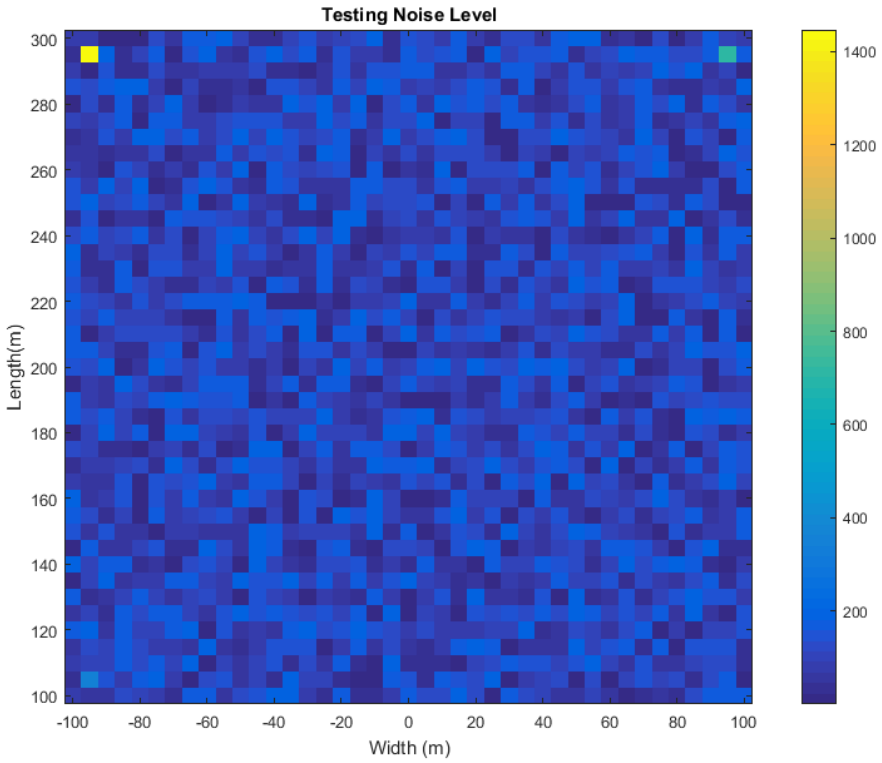

Figure 57: Testing the noise level using different scattering values at each corner of the scene.

As we could see, we are able to distinguish the scattering values of 1, 0.5 and 0.25 because they are over the noise level. But the scattering value of 0.125 is similar to the noise level so we are not able to distinguish it from the ones generated by the noise.

We know that the resolutions of our GEOSAR Radar would be approximately:

$$\Delta_r = \frac{C}{2B} = 5\ meters$$

$$\Delta_a = \frac{\lambda\rho}{2R_a} = \frac{\lambda\rho}{2\frac{\lambda H}{L\cos\theta}} = \frac{L}{2} \approx 13\ meters$$

So the main lobe of the focused image should have -3dB amplitude in both directions of 5 meters and 13 meters in range and azimuth directions respectively.

Let's see if that is true in our focused images. For doing that let's take the image of the scene with just one target on the middle of it, and let's take 2 cuts that contain the target, one cut in range and the other one in azimuth. The result is the next one:

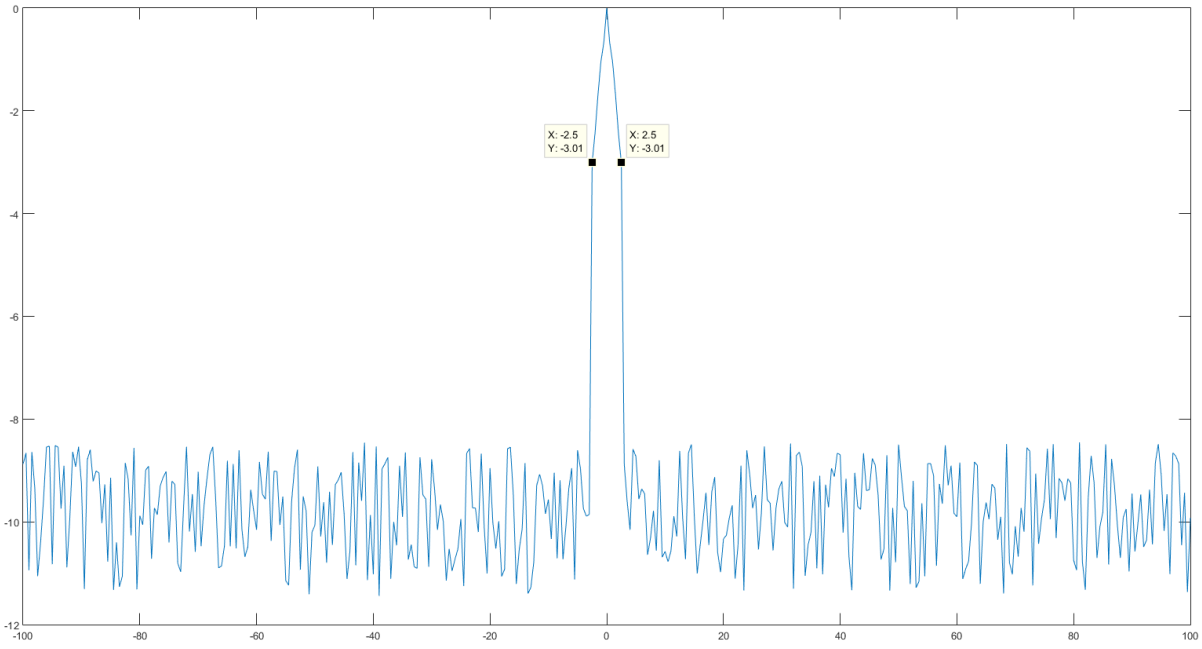

Figure 58: Range Resolution, taking a scene with 1 target placed in the middle of it.

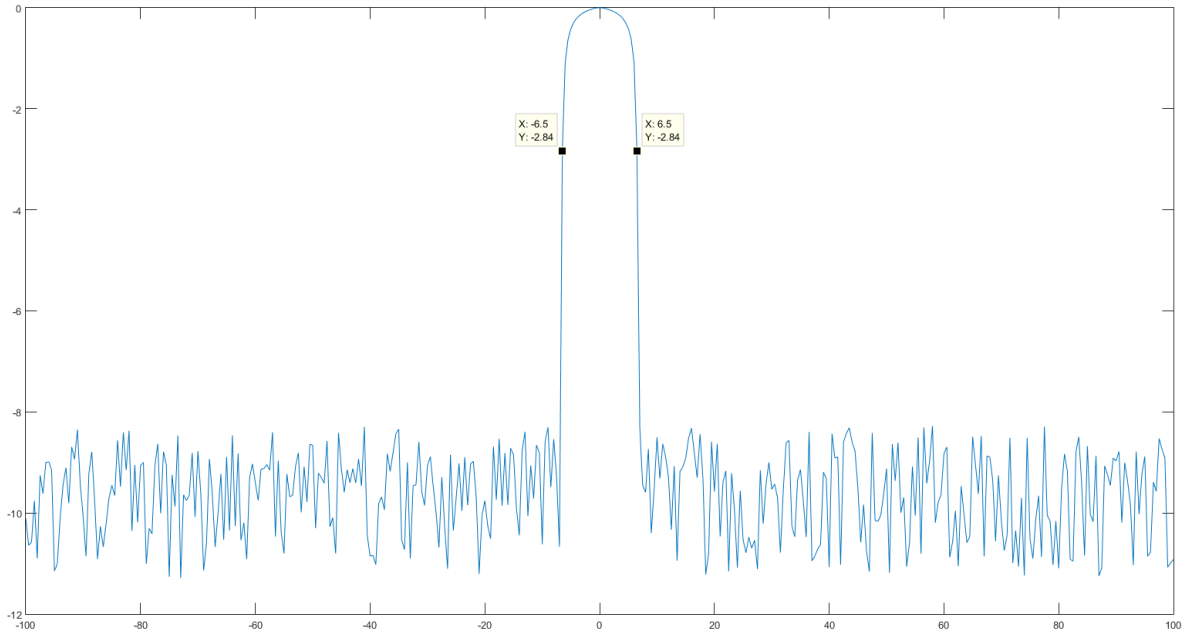

Figure 59: Azimuth Resolution, taking a scene with 1 target placed in the middle of it.

As we are able to see the both resolutions, range and azimuth, are very similar to the theoretical values. That proves that the simulation is working well and that it is possible to obtain SAR images with the expected resolution from a geostationary satellite.

7. CONCLUSIONS AND FUTURE WORK:

Thus, all along this thesis the most relevant features on how to perform a back projection algorithm on a bistatic GEOSAR system with on-ground receiver have been studied. Particularly, a program that is able to simulate the algorithm has been developed. This program works properly and gives us as an output some focused images obtained from a geostationary orbit.

Additionally, the focused images obtained from the simulated algorithm, have been analyzed in order to prove that the algorithm will be valid when it would have to be applied in a real GEOSAR system. As it has been proved in the previous section, it will accomplish all the requirements that an imaging system has.

This is just a little part of all the work that is being done in GEOSAR ambit. Tracking, orbital determination, system hardware development and other important aspects are being studied in parallel with the development of that thesis. The result of that thesis is very useful, but it will not be used until all the other aspects of the GEOSAR have been studied and physically realized. That is because the imaging part of a radar is the last part that should be implemented. It is the last block on the chain of imaging.

In the part of imaging future work should be done. For example, the code of the back projection algorithm is functional, but it is not efficient. Some work on making the code efficient, for example using the matrix-oriented behavior of MatLab.

Finally, using the algorithm with real data is the most important thing that should be done in the section of GEOSAR imaging in order to prove that the algorithm will work perfectly with real information.

REFERENCES:

[1] Curlander, J.C.; McDonough, R.N. *Synthetic Aperture Radar: Systems and Signal Processing.* New York, 1991.

[2] Tomiyasu, K., "Synthetic aperture radar in geosynchronous orbit," *Antennas and Propagation Society International Symposium, 1978,* vol.16, no., pp.42, 45, May 1978.

[3] Cumming, I.; Wong, F. *Digital Processing Of Synthetic Aperture Radar Data: Algorithms and Implementation*. Artech House Publishers, New York, 2005.

[4] Ruiz Rodon, J. *Study on the feasibility of geosynchronous satellites for synthetic aperture radar applications.* Master thesis, Universitat Politecnica de Catalunya (UPC).

[5] Soumekh, M. *Synthetic Aperture Radar Signal Processing with MATLAB Algorithms*. John Wiley & Sons, New York, 1999

[6] Guzmán Bofarull, M. Feasibility study of geosynchronous SAR satellites. Final degree thesis, Universitat Politecnica de Catalunya (UPC).

[7] Elachi, C. 'Spaceborne SAR Remote Sensing: Applications and Techniques', Chapters 3-5, IEEE Press, 1987.

[8] Tomiyasu, K.; 'Synthetic Aperture Radar Imaging from an Inclined Geosynchronous Orbit', Geoscience and Remote Sensing, IEEE Transactions on, vol.GE-21, no.3, pp.324-329, July 1983.

[9] Ze Yu; Jie Chen; Chunsheng Li; Zhuo Li; Yan Zhang; Concepts, properties and imaging technologies for GEO SAR. Proc. SPIE 7494, MIPPR 2009: Multispectral Image Acquisition and Processing, 749407 (October 30, 2009).

[10] Cheng Hu; Teng Long; Tao Zeng; Feifeng Liu; Zhipeng Liu; , 'The Accurate Focusing and Resolution Analysis Method in Geosynchronous SAR,' Geoscience and Remote Sensing, IEEE Transactions on, vol.49, no.10, pp.3548-3563, Oct. 2011.

[11] Liu Qi; Wei-Xian Tan; Yun Lin; Yan-ping Wang; Wen Hong; Yi-rong Wu; 'SAR raw data 2-D imaging model and simulation of GEOSAR', Radar (Radar), 2011 IEEE CIE International Conference on, vol.1, pp.833-386, 24-27 Oct. 2011.

[12] Zhipeng Liu; Di Yao; Teng Long; 'An accurate focusing method in GEOSAR', Radar Conference (RADAR), 2011 IEEE, pp.237-241, 23-27 May 2011.

[13] Li, Zhuo; Li, Chunsheng; Yu, Ze; Zhou, Jian; Chen, Jie; 'Back projection algorithm for high resolution GEOSAR image formation', Geoscience and Remote Sensing Symposium (IGARSS), 2011 IEEE International, pp.336-339, 24-29 July 2011.

[14] Zhipeng Liu; Cheng Hu; Tao Zeng; 'Improved Secondary Range Compression focusing method in GEOSAR', Acoustics Speech and Signal Processing (ICASSP), 2011 IEEE International Conference on, pp.1373-1376, 22-27 May 2011.

[15] M. Capderou, 'Satellites. Orbits and Missions', Chapter 2.3 Orbital Elements pp.51-55, 148-149, Springer, 2005.

[16] J.B. Tatum, 'Physics topics. Celestial Mechanics', Chapter 3: Plane and Spherical Trigonometry, Electronic Source.

[17] Curlander, J.C. and McDonough, R.N., 'Synthetic Aperture Radar: Systems and Signal Processing', Chapter 3: The matched filter and pulse compression, New York, 1991.

[18]Madsen, S.N., and Zebker, H.A. 'Imaging radar interferometry. Principles & Applications of Imaging Radar' (Manual of Remote Sensing (3rd ed.), vol2), New York: Wiley, 1998.

[19] Gustafsson, M,; Herberthson, M.; Rahm, J.; Zdansky, E.; Orbom, A.; 'A New Methodology for Measuring the Bistatic ground Scattering Coefficient Comparisons with the AIEM at Large Bistatic Angles', Geoscience and Remote Sensing Letters, IEEE, vol.10, no.5, pp.1167-1170, Sept.2013.

[20] Duersch, M. 'Backprojection for Synthetic Aperture Radar', Electrical and Computer Engineering Commons, June 2013.

[21] Duboshin, G.N. ; 'Celestial Mechanics: Basic Problems and Methods', Moscow, 1975.

[22] Rosborough, G.W. ; 'Satellite Orbit Perturbations', Texas University, Austin, 1986.